Getting the Basics Right: Preparing Alkaline Electrolytes for Electrochemical Applications

Raúl A. Márquez,[†] *Kenta Kawashima,*[†] *Yoon Jun Son,*[††] *Grace Castelino,*[†] *Nathaniel Miller,*[‡] *Lettie A. Smith,*[†] *Chikaodili E. Chukwuneke,*[†] *and C. Buddie Mullins*[†,††,§,§§,‖,*]

[†] Department of Chemistry, The University of Texas at Austin, Austin, Texas 78712, United States.

[††] McKetta Department of Chemical Engineering, The University of Texas at Austin, Austin, Texas 78712, United States.

[‡] Department of Geosciences, The University of Texas at Austin, Texas 78712, United States.

[§] Texas Materials Institute, The University of Texas at Austin, Texas 78712, United States.

[§§] Center for Electrochemistry, The University of Texas at Austin, Austin, Texas 78712, United States.

[‖] H2@UT, The University of Texas at Austin, Texas 78712, United States.

* Corresponding author: mullins@che.utexas.edu

Number of pages: 54

Number of figures and schemes: 25

Number of tables: 5

Table of Contents

Materials

Acid dilutions for cleaning and ICP-MS analysis were prepared using TraceMetal grade nitric acid (Fisher Scientific, 67 - 70%, Fe < 1 ppb). Unless specified, alkaline electrolytes were prepared from reagent-grade potassium hydroxide (Sigma Aldrich, flakes, 89.9% according to the certificate of analysis) and sodium hydroxide (Sigma Aldrich, pellets, 98% according to the certificate of analysis). Other varieties of KOH used in this study are shown in **Table S1**. Detailed elemental contents in the certificate of analysis were only available for the ultra-high purity (UHP) variety, potassium hydroxide hydrate (TraceSELECT) for trace analysis (99.995% metal basis), purchased from Honeywell Fluka. Nickel(II) nitrate hexahydrate (Thermo Scientific, Puratronic, 99.9985% metal basis) was used for Fe purification. Primary standard potassium hydrogen phthalate (Thermo Scientific, ACS grade, 99.95 – 100.05%) was used for alkaline electrolyte titrations. Ni foam (99.99%, 80 - 110 ppi) with a thickness of 1.6 mm was purchased from MTI Co. NiFe foam (2.5% Fe) with a thickness of 1.5 mm was purchased from Kunshan Electronic Materials Co. High-purity hydrochloric acid (Thermo Scientific, 99.999% metal basis) was used to prepare 3 M HCl solutions for Ni foam cleaning. All the electrolytes and acid dilutions were prepared with deionized (DI) water (18.2 MΩ·cm).

Table S1. KOH varieties used in this study and their compositions given by manufacturers

Reagent	Manufacturer	Code	Assay (wt. %)	Fe conc. (ppm)	Co conc. (ppm)	Ni conc. (ppm)
KOH (flake)	Sigma Aldrich	fl1	89.90	-	-	-
KOH (pellet)	Sigma Aldrich	pe1	86.45	-	-	-
KOH (pellet)	Thermo Scientific	pe2	85.00	-	-	-
KOH (UHP)	Honeywell	UHP	99.40[†]	< 0.05	< 0.01	< 0.01
NaOH (pellet)	Sigma Aldrich	-	98.00	-	-	-

[†]Not metal basis. Considering the 0.6% of carbonate from the assay composition.

S1: Best Practices for Preparing Alkaline Electrolytes

We have implemented the following procedures to refine alkaline electrolyte preparation and improve analytical quality controls. These recommendations can be found in well-established chemical analysis textbooks.[1,2] All our electrolytes were prepared following these recommendations. We encourage future studies to follow these guidelines to ensure consistent and comparable results.

- ✓ CO_2 absorption deteriorates alkaline electrolytes by increasing the effective molarity (due to the formation of HCO_3^- and CO_3^{2-} ions).[3] Thus, CO_2 must be removed from the DI water to prepare alkaline electrolytes. The most convenient method is to boil DI water in a Florence flask covered with an inverted beaker and then cool it under cold water or overnight. This CO_2-free DI water can be stored in clean polypropylene (PP) bottles wrapped with Parafilm^{TM} until further use. Additionally, CO_2 can be removed from NaOH electrolytes by precipitating Na_2CO_3 from 50 wt.% NaOH (~19 M) solutions. Na_2CO_3 settles down after several days, and then the supernatant is decanted. Next, the carbonate-free NaOH is diluted until the desired concentration with CO_2-free DI water and standardized *via* titration. Note: this method does not work with KOH because K_2CO_3 remains soluble. For more details, we recommend reading Section 2.5 and Experiment 7 of Ref. 1. Once CO_2 is removed, avoid exposing the electrolytes to air as much as possible (*e.g.,* by leaving the solutions in closed plastic bottles instead of electrochemical cells or beakers). We also recommend regularly standardizing the electrolytes with a primary standard (see **Section S3**).
- ✓ We recommend sparging electrolytes with inert gases (*e.g.*, N_2, Ar) to displace other gases that could interfere with electrochemical tests. For example, O_2 should be removed when electrodepositing Fe or Co to prevent the oxidation of Fe^{2+} or Co^{2+} ions in the solution.[4] In

other cases, bubbling O_2 or H_2 is necessary to perform studies of gas evolution reactions. Note that care must be taken in removing bubbles from the surface of the electrodes.[5]

- ✓ KOH and NaOH are highly hygroscopic; therefore, they will absorb moisture when exposed to the atmosphere. Depending on the degree of accuracy, several strategies can be implemented, *e.g.,* working in cleanrooms or glove boxes with controlled humidity or drying solids before use. However, we note that not all researchers have access to such facilities, or the desired degree of accuracy may not be the same. Thus, we recommend weighing hygroscopic solids as quickly as possible. Store hygroscopic solids and primary standards in environments free of moisture (*e.g.,* desiccators). Note that the weight of a given amount of alkali is not reproducible, and the actual "purity" can vary significantly. Therefore, we encourage standardizing final alkaline electrolytes using primary standards. Standardizing alkaline electrolytes is the best (and most convenient) way to determine accurate alkali concentrations and compare reproducibility between operators and research groups.
- ✓ As we experimentally demonstrate in this study, the elemental composition and purity of alkali solids vary significantly from companies and types (*e.g.,* flakes, pellets). Thus, we recommend acquiring the certificate of analysis (COA) from the company website to use the absolute alkali purity (typically from chemical assays) when calculating the required alkali weight (Note: do not assume a chemical is 100% pure unless stated by COA). We have found that the purity varies even among different lot numbers, although the alkali is typically sold with a nominal purity (*e.g.*, 85 wt.%). Even if standardized against a primary standard, using the absolute purity given by the COA ensures that the final concentration remains as close as possible to the target molarity, reducing the variability when solutions are made using different lot numbers or by different operators.

- ✓ Wash electrochemical cells and their components with acids to remove adsorbed impurities, particularly metals. For example, graphite and Pt counter electrodes can be immersed in 5 M HNO_3 overnight or dipped for a few minutes in aqua regia.[4,6–9] Then, wash with copious amounts of DI water. Before use, cells and components can be rinsed with small amounts of electrolyte to remove the remaining DI water and prevent electrolyte dilution.
- ✓ Alkalis, especially hot solutions, attack borosilicate and soft glasses. As demonstrated in this study, using glassware increases Si, B, and Al concentrations in the alkaline electrolyte, which may affect the reproducibility or even the electrochemical performance of certain electrocatalysts.[10] Thus, avoid using glassware as much as possible when preparing/handling alkaline electrolytes. If plasticware is not readily available, use glassware as quickly as possible (*e.g.*, use volumetric flasks *only* to reach the mark, solids must be dissolved first in a beaker, see the next recommendation). A detailed summary of the properties of laboratory materials is shown in Table 2.1 of Ref 1.
- ✓ Because the dissolution of alkali solids in water is an exothermic process, solids must first be slowly dissolved in beakers, adding small amounts of solid and DI water while stirring the solution to dissipate heat. This routine can be done using plastic beakers and mixing rods or stir bars coated with polytetrafluoroethylene (PTFE). Never use volumetric flasks to dissolve the solid nor store the electrolyte because these actions deteriorate glassware/plasticware accuracy. Once the mixture cools down to room temperature, it can be transferred to a volumetric flask to reach the desired volume. Beakers (and stir bars/rods) can be washed several times with DI water at room temperature, which later can be used to fill the volumetric flask up to the mark. Note that reaching the mark needs to be done at the

right temperature (typically 20 ºC, depending on the volumetric flask) because the liquid density varies with temperature.

- ✓ Incorrect use of glass and plasticware can change their accuracy. Therefore, volumetric flasks, pipettes, and burettes must be regularly calibrated. Calibration by comparing the volume and weight of DI water at a constant temperature is the simplest and most convenient method, and it can be found in most analytical chemistry textbooks.[1,2]
- ✓ Only a few studies have reported using electrochemical cells made of PTFE or polypropylene (PP) vessels,[4,7,9–15], which are chemically inert and inexpensive. As we did for our electrochemical tests, PTFE cells can be easily made from hydrothermal reactor vessels. Although the most notable disadvantage is that these cells are not transparent, this should not be a problem if working at low current densities when bubble dissipation is not an issue. PTFE cells can also be adapted to incorporate visualization windows made of acrylic if necessary. We strongly encourage using glass-free cells and components when using alkaline electrolytes, especially at high concentrations or during prolonged operation.
- ✓ Always use trace metal-grade acids (HNO_3, HCl, H_2SO_4) for cleaning and rinsing cells, components, and containers for storing and purifying electrolytes. Nitric acid must be used for ICP-MS analysis to avoid contamination of Cl and S. For ICP-MS analysis, always examine the blank composition for possible contamination to avoid a systematic error.

S2: Fe Purification Routine

We adapted the well-known Fe purification routine proposed by Trotochaud *et al.*[9] by optimizing certain steps and providing more specific details to standardize the procedure. **Scheme S1** shows a detailed workflow of all the steps, described as follows.

About 2 g of high-purity (> 99.99%) nickel nitrate hexahydrate are dissolved in 4 mL of DI water inside a 50 mL polypropylene centrifuge tube. First, the tube is vigorously shaken in a vortex mixer until the salt is completely dissolved. Next, 20 mL of unpurified 1 M KOH electrolyte are added, resulting in insoluble $Ni(OH)_2$. Then, the tube is sonicated in an ultrasonic bath for at least 10 min and then shaken in a vortex mixer. The tube is centrifuged at 8000 rpm for 10 min, and then the supernatant is slowly decanted. Next, three washing cycles are performed by adding 20 mL of DI water and 2 mL of KOH electrolyte, sonicating, redispersing the solid using the vortex mixer, centrifuging, and decanting the supernatant. Then, the precipitate is carefully rinsed three times with 5 mL of unpurified electrolyte (without redispersing the solid) to remove residual DI water from the washing cycles. Next, 30 mL of unpurified electrolyte are added, and the solid undergoes two redispersing cycles by shaking in the vortex mixer for 5 min and sonicating for 10 min. At this point, the precipitate should disintegrate into fine particles, and large $Ni(OH)_2$ chunks should not remain in the suspension (more cycles may be needed). Finally, 20 mL of electrolyte are added to complete a total of 50 mL, and the tube is left for at least 48 h of resting until all the solid phase settles down. After resting, the tubes are centrifuged at 10,000 rpm for 10 min, and the supernatant is decanted. To avoid carrying small $Ni(OH)_2$ particles, the supernatant is filtered with a disposable polyethersulfone membrane filter (Thermo Scientific, Nalgene 0.1 μm PES) fitted to a 60 mL polypropylene syringe. The filtered electrolyte is received in a clean PP bottle for storage.

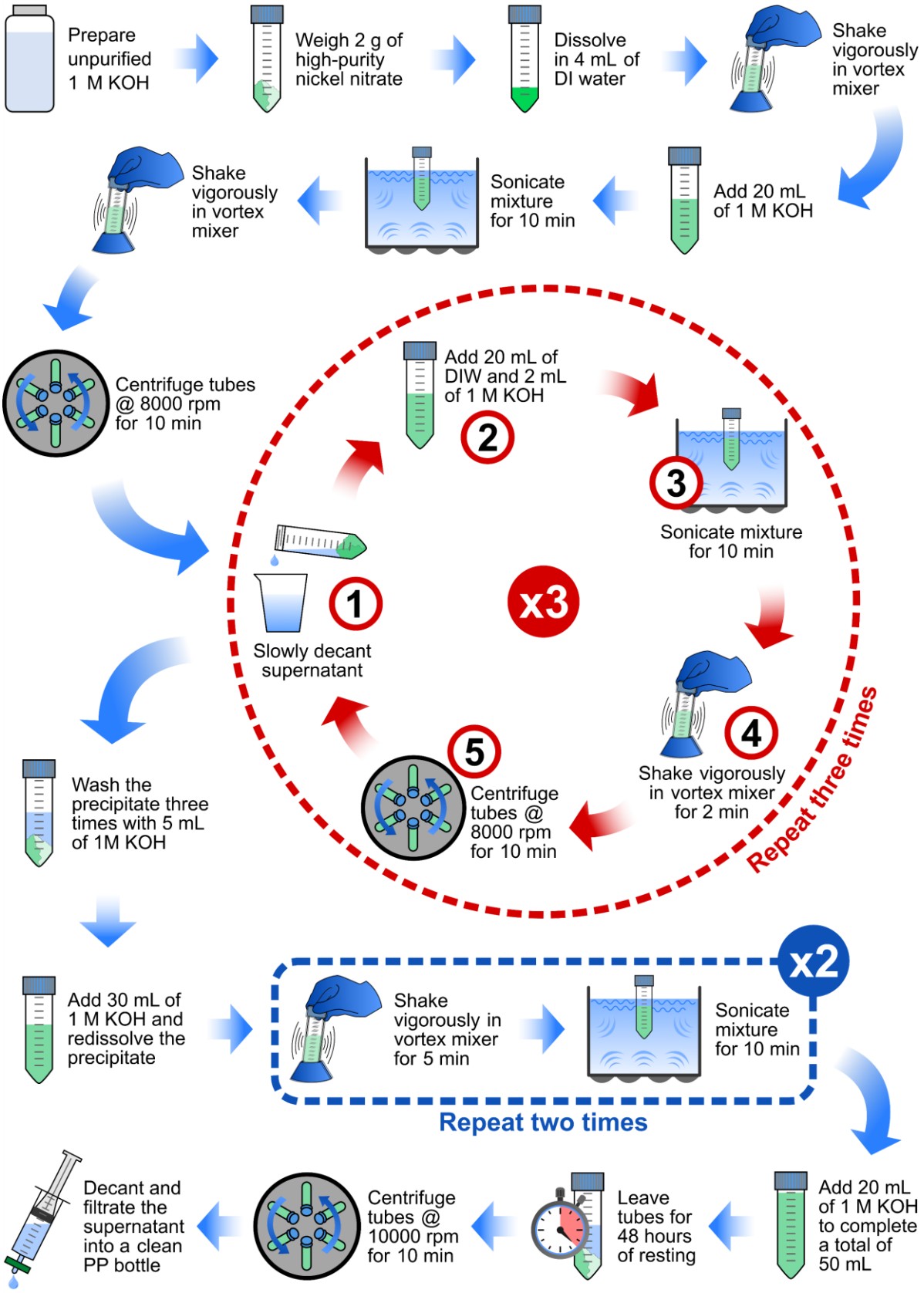

Scheme S1. Suggested workflow for alkaline electrolyte purification.

In our experience, adding extra steps to the routine proposed by Trotochaud *et al.*[9] improves the quality of the purified electrolyte. Specifically, we note that:

- ✓ Centrifuge tubes, polypropylene bottles, and plastic syringes must be rinsed with 3 M HNO_3 and copious DI water to remove trace metals. Nitric acid solutions must be prepared from high-purity nitric acid. Although other acids can be used (e.g., H_2SO_4), care must be taken as S, and Cl traces may interfere when the electrolyte is analyzed *via* ICP-MS.
- ✓ Redispersing the solid using the vortex mixer and sonication improves the fragmentation of insoluble $Ni(OH)_2$ particles, increasing the contact area with the electrolyte and absorbing Fe more effectively. These steps are also crucial during washing cycles to maximize the formation of the $Ni(OH)_2$ phase. In general, systematical re-dispersion of the precipitate results in enhanced purification and improved reproducibility.
- ✓ Washing the precipitate three times with electrolyte before adding 50 mL ensures water is completely removed, so the final Fe-purified electrolyte is not diluted (see **Figure S5**).
- ✓ In the final stage of the routine, redispersing the solid phase in 30 mL instead of 50 mL of electrolyte makes solid fragmentation easier and more effective due to the headspace and air bubbles that increase the turbulence when shaking in the vortex mixer. After redispersing the solid, 20 mL are added to complete 50 mL and maximize the amount of purified KOH.
- ✓ Filtering the supernatant in the final step prevents insoluble $Ni(OH)_2$ particles from entering the purified electrolyte, as shown previously by Liu and coworkers.[16] Filtration using nanoporous syringe filters, such as hydrophilic 0.1 μm polyethersulfone (PES) filters, decreases Fe, Ni, and Co concentrations below 10 ppb. Filtering is essential when studying Ni dissolution, as $Ni(OH)_2$ particles from the purification routine could increase the Ni concentration in the electrolyte.

- ✓ PES filters must not be reused when filtering the electrolyte supernatant since air typically clogs the filter. Filtering must be done slowly to avoid breaking the filter.
- ✓ Large and clean plastic syringes (~50 mL) are recommended to maximize the amount of filtered electrolyte.
- ✓ We recommend scaling up the mass of nickel nitrate hexahydrate based on the electrolyte concentration, as concentrations >1 M would contain more Fe, and ~2 g would not be effective in removing Fe (see **Figure S9b**).

S3: Volumetric and pH Titrations of Alkaline Electrolytes

The weak acid – strong base volumetric titration is a well-known and established method for standardizing alkaline electrolytes.[1,2] Volumetric titration using potassium acid phthalate (KHP) as primary standard is simple and convenient because KHP can be weighed accurately (it is not hygroscopic). This method uses a burette to add precise amounts of the alkaline electrolyte to a known weight of KHP dissolved in CO_2-free DI water. The endpoint of the titration can be determined utilizing a phenolphthalein indicator or by following the change in pH *via* a calibrated pH meter.[1] The procedure utilized in this study is described as follows:

KHP is dried overnight in a vacuum oven at 60 ºC. Then, KHP is cooled in a desiccator for at least 30 min before weighing. Approximately 1 g of KHP is weighed, and the mass is fully dissolved in ~50 mL of CO_2-free DI water using a PTFE magnetic stir bar. We use a PTFE vessel specifically for alkaline electrolyte titrations (the experimental setup is shown in **Figure S1**). A 25 mL acrylic-body burette with PTFE stopcocks (Thermo Scientific Nalgene, graduation interval: 0.1 mL, tolerance: ±0.06 mL, calibrated to meet ASTM E287 requirements) is (1) washed with 3 M HNO_3, (2) rinsed with copious DI water three times, (3) rinsed with the alkaline electrolyte to standardize, and (4) filled up to the 25 mL mark with alkaline electrolyte. Next, a few drops of phenolphthalein indicator (~0.5 g dissolved in 50% ethanol/water solution) are added to the KHP solution. The sample is titrated by adding small increments of alkaline electrolyte under vigorous stirring. The endpoint of the titration is tracked simultaneously by recording the pH using a pH meter (Fisher Scientific, Accumet AB15) and the color change given by the indicator (*i.e.*, when the solution turns colorless to pink). The volume of alkaline electrolyte associated with the endpoint is used to calculate the molarity, as it corresponds to the moles of alkali required to neutralize the moles of KHP.

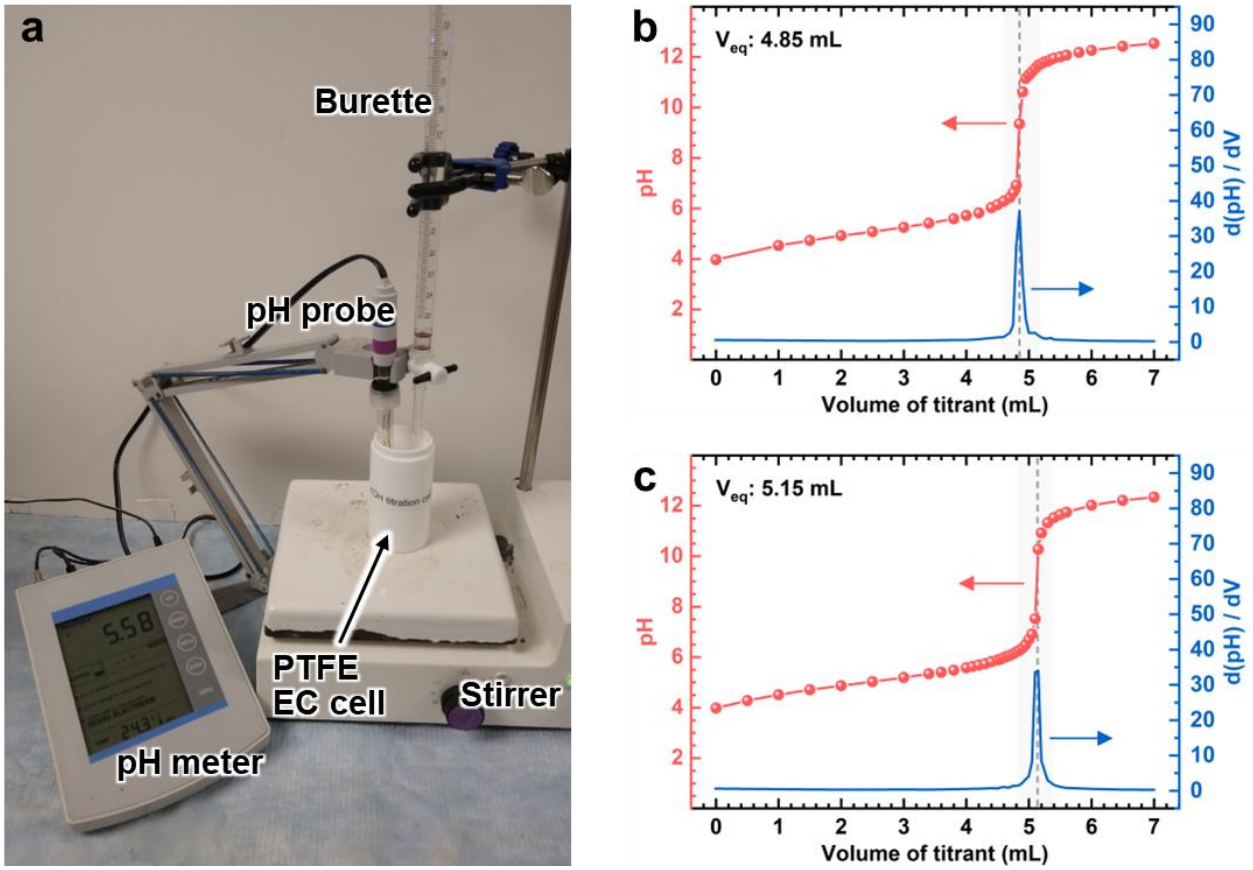

Figure S1. Standardization of alkaline electrolytes through acid-base titrations: (a) experimental setup of the coupled volumetric/pH titration routine; titration curves showing the volume of titrant against the pH (left axis, red) and the first derivative of the pH curve (right axis, blue) using (b) ~1 M KOH and (c) ~1 M NaOH as titrants.

We provide a spreadsheet to ease the calculation of molarities using this method. The spreadsheet is devised to standardize KOH and NaOH electrolytes with concentrations close to 1 M using primary standard KHP (~1 g). The spreadsheet includes calculations for volumetric titrations using phenolphthalein as indicator and pH titrations. When volumetric titrations are done, the operator only needs to specify the KHP purity, the mass of KHP dissolved in DI water, and the volume of base necessary to reach the equivalence point. In addition, the spreadsheet includes a pH titration tab containing tables to construct pH titration curves. The volume of titrant (base) added is automatically plotted against the measured pH, and the equivalence point

can be determined at the curve's inflection point. Volume intervals have already been specified to improve the shape of the pH titration curve near the inflection point. Moreover, the first derivative of this curve d(*pH*)/d*V* is also plotted against the volume of titrant because the first derivative curve shows a maximum at the equivalence point. Both curves can be used to determine the volume of base necessary to neutralize the moles of KHP and therefore estimate the molarity of the solution. **Figures S1b** and **c** show pH titration curves for ~1 M KOH and NaOH, respectively.

We suggest the following strategies for improving titrations of alkaline electrolytes:

- ✓ Instead of drying overnight under vacuum, KHP can be alternatively dried quickly in a weighing bottle at 120 ºC for 2 h. KHP must be cooled in a desiccator before weighing.
- ✓ KHP should always be dried, stored, and carried in weighing bottles to avoid contamination.
- ✓ Cleaning the burette with acid and deionized water is essential to neutralize and remove the remaining alkali from previous titrations. Pre-conditioning with a few mL of the base also helps to remove the remaining water and prevent incidental dilution of the base.
- ✓ When using a pH probe, it is recommended to wait until the pH reading is stable. Vigorous stirring with a magnetic stir bar significantly improves mixing and reduces measuring time.
- ✓ pH probes must be calibrated through a three-point calibration routine according to the manufacturer.
- ✓ We recommended standardizing alkaline electrolytes right after preparation to estimate the initial molarity. The molarity can be tracked daily, weekly, or monthly, depending on its exposure to CO_2 or after specific tests to use a correct pH to plot electrochemical data.

S4: Solution-mode ICP-MS Analysis

We developed a solution-mode inductively coupled plasma mass spectrometry (ICP-MS) method to determine the elemental composition of the alkaline electrolytes. Based on previous approaches for analyzing KOH electrolytes,[17,18] we devised a procedure to dilute concentrated alkaline electrolyte samples (~1 M) with ultra-high purity water and trace metal-grade 2% nitric acid, as depicted in **Scheme S2**. The challenging matrix with high total dissolved solids contents (mainly K^+ and Na^+) is diluted to ensure instrument stability and improve plasma performance while the detection limits of all the analytes stay in the low ppb range.

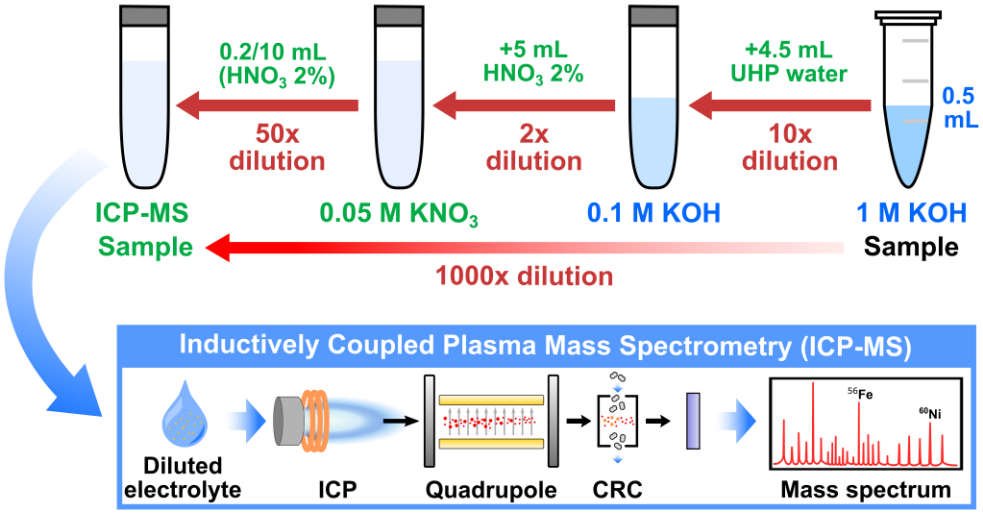

Scheme S2. Dilution routine used for electrolyte analysis *via* solution-mode ICP-MS.

The instrument consisted of an Agilent 7500ce inductively-coupled plasma mass spectrometer equipped with a quadrupole mass analyzer and a collision/reaction cell (CRC). The method was optimized by tuning the plasma in no gas, He, and H_2 modes to remove unwanted polyatomic interferences. We also examined the accuracy and precision of the method by analyzing quality control and spiked samples prepared from reference standards and obtained calibration curves for the analyzed isotopes. The complete analytical procedure, experimental

setup, quality control routines, and results from two previous analytical projects are detailed in the following website from the Jackson School of Geosciences, UT Austin:

https://www.jsg.utexas.edu/geo392-f21-class-project-group-vf50otr6gr/

Table S2 summarizes the performance metrics of the ICP-MS method, including the optimal gas modes for each analyte, the coefficient of determination from each calibration curve, the recoveries of three different quality controls, the limit of detection (LOD), determined as the product of the standard deviation of each m/z signal and the t-value (95% confidence) from 20 replicates of the blank, and the practical quantitation limit (PQL) determined as ten times the standard deviation of each m/z signal. Except for those elements with high concentrations in the alkaline electrolyte (*i.e.*, Na, Si, P, K, and Ca), all the analytes exhibited LODs below 1 ppb.

In addition to determining the elemental composition of as-prepared alkaline electrolytes, we have demonstrated the robustness of this ICP-MS method to examine the metal dissolution of 3D-printed electrodes in alkaline media during the OER.[19] Thus, we recommend using or adapting this method for examining the composition of alkaline electrolytes during relevant electrochemical processes, mainly gas evolution/reduction reactions that strongly rely on KOH and NaOH electrolytes. Furthermore, previous studies have demonstrated that solution-mode ICP-MS is a powerful and reliable tool that can be used to track elemental dissolution/re-deposition processes,[13,20–25] which are essential for understanding the dynamic stability of different electrocatalysts.[13,26] We strongly advocate using elemental analysis techniques with high sensitivity, like ICP-MS, to analyze alkaline electrolytes. These techniques would strengthen the claims of "impurity-free" systems in this field, complementing typical characterization using X-ray photoelectron spectroscopy or energy-dispersive X-ray spectroscopy (EDX) where sensitivity could be insufficient.[7,11,27]

Table S2. Metrics for solution-mode ICP-MS method evaluation

m/z	Analyte	Mode	R^2	Q1 Rec.	Q2 Rec.	Q3 Rec.	LOD (ppb)	PQL (ppb)
7	**Li**	ng	1.0000	1.04	0.99	1.05	0.04	0.20
11	**B**	ng	0.9999	0.93	0.93	0.89	0.40	1.88
23	**Na**	ng	1.0000	1.01	0.99	1.01	6.82	32.60
24	**Mg**	He	1.0000	1.03	1.11	1.08	0.21	1.02
27	**Al**	ng	1.0000	1.05	1.04	1.12	0.91	4.34
28	**Si**	H_2	0.9997	1.03	1.03	-	5.14	24.57
31	**P**	ng	1.0000	0.97	0.98	-	3.17	15.16
39	**K**	He	1.0000	1.04	1.10	1.09	28.85	137.86
40	**Ca**	H_2	1.0000	1.04	1.04	1.01	3.85	18.41
47	**Ti**	ng	1.0000	1.01	1.09	-	0.01	0.06
51	**V**	He	1.0000	1.02	1.00	0.98	0.01	0.04
52	**Cr**	He	1.0000	1.05	1.02	1.00	0.02	0.08
55	**Mn**	ng	0.9999	1.07	1.06	1.07	0.01	0.05
56	**Fe**	He	1.0000	1.06	1.04	1.03	0.06	0.30
59	**Co**	ng	0.9999	1.02	1.00	1.01	0.01	0.03
60	**Ni**	ng	1.0000	1.02	1.03	1.02	0.01	0.04
63	**Cu**	ng	0.9999	1.04	1.07	1.04	0.01	0.04
66	**Zn**	ng	0.9998	1.05	1.05	1.08	0.04	0.18
75	**As**	He	1.0000	0.97	0.97	0.99	0.03	0.13
78	**Se**	H_2	1.0000	1.06	1.02	1.04	0.03	0.13
85	**Rb**	ng	0.9999	1.07	0.94	1.04	0.01	0.03
88	**Sr**	ng	1.0000	1.01	1.02	1.03	0.05	0.22
90	**Zr**	ng	1.0000	0.96	0.99	-	0.01	0.03
95	**Mo**	ng	0.9999	0.99	0.97	0.98	0.37	1.78
107	**Ag**	ng	0.9999	1.07	0.99	-	0.01	0.04
114	**Cd**	ng	1.0000	0.96	0.96	0.94	0.01	0.03
118	**Sn**	ng	1.0000	1.02	1.02	-	0.01	0.03
121	**Sb**	ng	0.9999	0.93	0.93	0.93	0.01	0.03
133	**Cs**	ng	1.0000	1.04	1.03	-	0.01	0.03
137	**Ba**	ng	1.0000	1.00	0.98	0.99	0.01	0.06
205	**Tl**	ng	0.9998	1.06	1.04	1.06	0.01	0.04
208	**Pb**	ng	0.9999	1.05	1.03	1.05	0.01	0.04
209	**Bi**	ng	0.9997	1.10	1.07	1.06	0.01	0.05
232	**Th**	ng	1.0000	1.00	0.25	-	0.01	0.03
238	**U**	ng	0.9999	0.97	0.92	-	0.01	0.03

ng: no-gas mode, Rec: recovery, LOD: limit of detection, PQL, practical quantitation limit

S5: Statistical Quality Control

Determining and reporting statistical metrics is essential. To assist in this endeavor, the spreadsheet automatically provides statistical metrics for electrolyte standardization. Descriptive statistics, including the mean, standard deviation, and relative standard deviation (RSD), are provided for two to six replicates. We arbitrarily set an RSD limit of 5% to determine if the repeatability of the molarity estimation is reliable, although the operators can set this limit. Standard uncertainties at 95% and 99% confidence are also automatically estimated when two or more replicates are performed. Confidence intervals can be used to express the uncertainty range of the solution and therefore compare molarities. An excellent description of uncertainties can be found in Refs. [28] and [29].

Descriptive statistics are also used to construct control charts (also known as Shewhart charts) to monitor changes in the molarity from the initial value.[30] If the molarity at a particular time falls outside the *action lines* or two successive molarities are outside the same *warning line*, the molarity is judged to be out of control. This means that the molarity likely changed due to significant absorption of CO_2 or incidental dilution during handling, and the electrolyte needs to be standardized again (or discarded if needed). Finally, the Grubbs' test for outliers is automatically calculated to identify replicates that significantly deviate from the others. If a trial is considered an outlier, it must be discarded and repeated. More details about these statistical concepts can be found in Ref. [30]. Although this spreadsheet was initially devised for ~1 M alkaline electrolytes and ~1 g KHP, operators can easily modify the volume intervals and titration tables to analyze other molarities or change the primary standard. Note also that this spreadsheet is only designed for monoprotic titrations (*i.e.*, single equivalence point). The equations need to be updated if polyprotic acids and bases are used.

S6: Electrochemical Methods

Electrode Preparation

Ni foam pieces (20 × 10 × 1.6 mm) were cut, and half of the piece was flattened out using nylon-coated jaw pliers, leaving intact a 10 × 10 × 1.6 mm square (acting as the electrode active area, see **Figure S2b** in the next section). Next, the pieces were washed in ethanol inside shell type 1 glass vials (15 × 45 mm, Fisher Scientific), placed in an ultrasonic bath for 15 minutes, and dried overnight in a vacuum oven at 60 ºC. The exposed electrode surface area was fixed using a polydimethylsiloxane (PDMS) coating (SYLGARD 184 Silicone Elastomer Kit, Dow). The coating was prepared by vigorously mixing the curing elastomer base and the curing agent in a 10:1 ratio for 10 min using a PTFE rod. Next, the mixture was degassed for ~5 min in a vacuum oven until no bubbles were seen. The liquid mixture was applied over ~5 mm on the compressed part, right next to the active area. The remaining 5 mm flat area was left uncovered to act as the clipping part. The PDMS-coated Ni foam pieces were placed on weighing paper sheets and over a metallic tray for curing in a small oven. The Ni foam pieces were folded such that the PDMS never touched the weighing paper. The PDMS-coated electrodes were cured at 150 ºC for 10 min as recommended by the manufacturer. After curing, the electrodes were kept in a vacuum oven until use. Before electrochemical measurements, the PDMS-coated electrodes were placed inside clean shell type 1 vials and cleaned sequentially using the following solutions while in an ultrasonic bath for 15 min each: (1) ethanol, (2) 3 M HCl, and (3) DI water. After clipping the electrode to a Ti clip holder, the active area was wetted with some 1 M KOH solution using a small wash bottle to remove air pockets from the porous matrix.

Electrochemical Measurements

Electrochemical tests were performed in a PTFE cell to avoid contamination from glassware. As shown in **Figure S2a**, the cell consisted of a 100 mL PTFE vessel originally intended for hydrothermal synthesis. Three ¼" holes were drilled in the cap to fix ¼" male nylon fittings, which served as electrode connection ports. All the components were cleaned before experiments with 3 M HNO_3 and rinsed with copious DI water. Electrochemical measurements were conducted using a Gamry Reference 620 potentiostat/galvanostat in three-electrode mode. A graphite rod (Gamry) was used as a counter electrode to avoid incidental Pt incorporation.[31] The counter electrode was cleaned periodically by soaking in 3 M HNO_3. Fresh and clean rods were used for ultra-high purity (UHP) and Fe-purified KOH measurements.

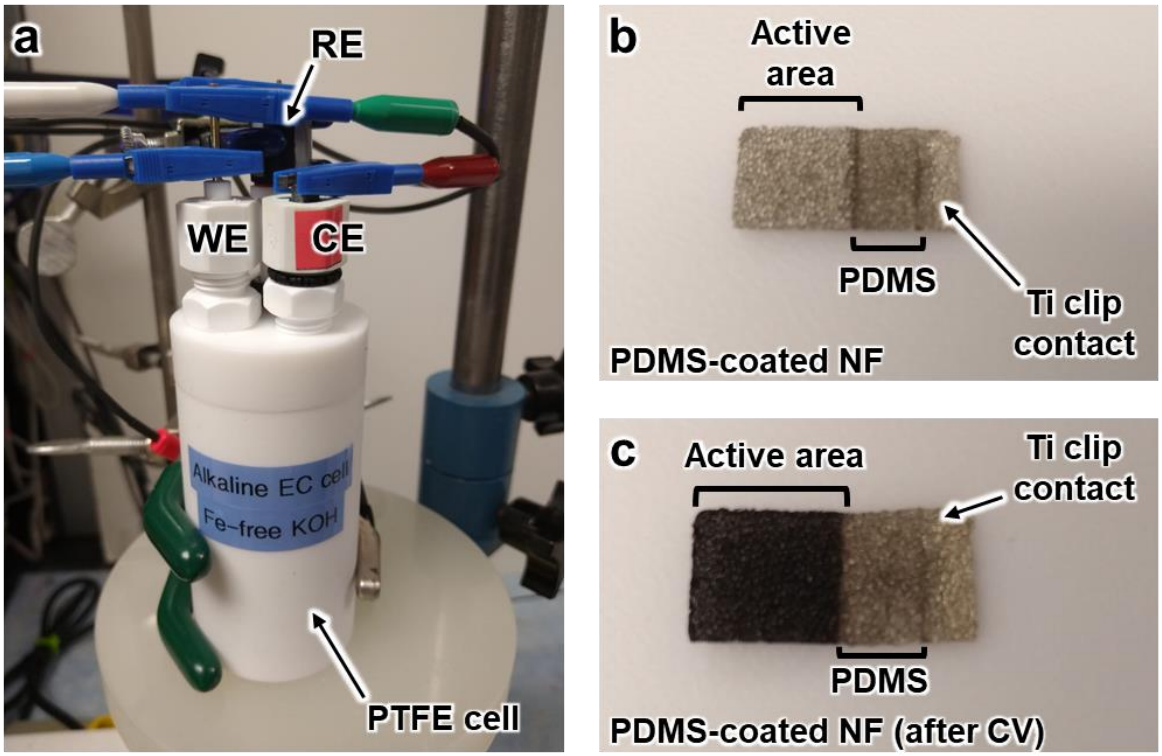

Figure S2. Electrochemical testing of Ni foam electrodes for validation of alkaline electrolytes: (a) photo depicting the three-electrode PTFE electrochemical cell used in this study, (b) PDMS-coated Ni foam electrode with 1 cm^2 exposed area, (c) PDMS-coated Ni foam electrode after extended CV testing, confirming that only the 1 cm^2 exposed area was oxidized during EC tests without electrolyte penetration due to PDMS blockage.

All potentials were measured against a Hg/HgO reference electrode with the same electrolyte as the filling solution (CH Instruments). Potentials were converted to the reversible hydrogen electrode (RHE) according to the equation ($E_{\mathrm{RHE}} = E^{\circ}_{\mathrm{Hg/HgO}} + 0.0592 \times \mathrm{pH} + E_{\mathrm{i}}$), where E_{i} is the measured potential *vs.* Hg/HgO. The values of $E^{\circ}_{\mathrm{Hg/HgO}}$ for ~1.0 M KOH and ~1.0 M NaOH Hg/HgO reference electrodes were measured experimentally to be 0.109 and 0.107 V (± 2 mV variation) by checking against a saturated calomel electrode used only for this purpose. In addition, the potential of the Hg/HgO reference electrode was periodically checked against a second Hg/HgO electrode to ensure stability between experiments.

We use a standard hydrogen electrode (SHE) to calibrate the saturated calomel electrode and correct for potential drift between measurements.[32] The SHE can be made using a platinized Pt electrode in acidic electrolyte having a unit activity of H^+ and $H_{2,(g)}$ (1 bar). The reversible potential for hydrogen is estimated as the average between forward and reverse sweeps around the potential of zero current. More details can be found elsewhere.[32–34]

Fresh electrolytes were used for each electrochemical test, and five replicate measurements were done. Electrolytes were degassed with high-purity O_2 for 30 min before measurements using a plastic bubbler. Due to reproducibility concerns, we used magnetic stirring to dislodge bubbles for 15 to 30 min only after degassing the electrolyte but not during electrochemical tests. The open circuit potential (OCP) was measured simultaneously (60 min), and experiments were performed only after the potential was completely stable (between -0.05 and -0.15 V *vs.* Hg/HgO, ±5 mV variation). Linear sweep voltammetry (LSV) and cyclic voltammetry (CV) scans to compare the samples before and after activation were recorded at a scan rate of 5 $\mathrm{mV \cdot s^{-1}}$ to minimize capacitive contributions, whereas CV scans used for extended activation were recorded at 50 $\mathrm{mV \cdot s^{-1}}$. CV scans were performed between 0.15 and 0.80 V *vs.* Hg/HgO for

purified electrolytes and 0.15 and 0.70 V *vs.* Hg/HgO for unpurified electrolytes. The third scan is reported for LSV and CV scans recorded before and after activation. For CV activation, scans are reported every 5, 100, 200, 400, 800, 1200, 1600, and 2000 cycles.

Electrochemical data were corrected for uncompensated resistance (R_u) using the positive-feedback mode in the Gamry software. LSV and CV scans were corrected for 85% of the R_u, measured from the minimum of total impedance at high frequencies (between 80 and 30 kHz) measured at 0.0 V *vs.* Hg/HgO and an amplitude of 5 mV, where the phase angle is near zero, and capacitive and inductive impedances are negligible.[4,9] The value of R_u varied from 1.5 to 1.9 Ω for Ni foam electrodes. R_u was monitored periodically among experiments to ensure good contact with the Ti clip electrode (variation was ~0.02 Ω).

Potentiostatic electrochemical impedance spectroscopy (EIS) tests were performed to find the charge transfer resistance (R_{ct}) associated with the OER and the double-layer capacitance (C_{dl}). EIS was measured in the frequency range from 0.15 to 10^6 Hz at an amplitude of 5 mV. Potentials in the 0.60 to 0.75 V *vs.* Hg/HgO range were probed to achieve similar current densities before and after extended CV activation.[15] EIS fitting was performed using the general Randles equivalent circuit model, and fitted parameters were determined using the Gamry Echem Analyst software. Please refer to **Supporting Note 5** for more information about EIS fitting. The overpotential (η) was calculated using the equation $\eta = E_i - E_{rev}$ where E_i is the measured potential (corrected for 85% R_u) and E_{rev} is the reversible potential of the OER (0.306 V *vs.* Hg/HgO).[7] All the current densities were calculated from a projected geometric area (1 cm^2) defined by the PDMS coating (**Figure S2b**). This coating effectively prevented the electrolyte from penetrating the flat area due to capillary action. As shown in **Figure S2c**, only the 1 cm^2 area was converted into active Ni oxide/hydroxide during CV activation. In contrast,

the rest of the flat Ni foam remained unchanged. More details about the reasoning behind PDMS and the geometric area instead of the total surface area are explained in **Supporting Note 1**.

Material Characterization

Scanning electron microscopy (SEM) was conducted to observe the morphology of the NiFe electrode using a FEI Quanta 650 microscope. Images were taken using a spot size of 4 nm and 20 kV. In addition, EDX was performed to obtain elemental mappings. The percent of each element shown in **Figure S20b** corresponds to the average of three different spots on the surface of the sample. For samples analyzed after electrochemical tests, the electrodes were dried overnight in a vacuum oven at 60 ºC before SEM and EDX measurements.

Supporting Figures and Tables

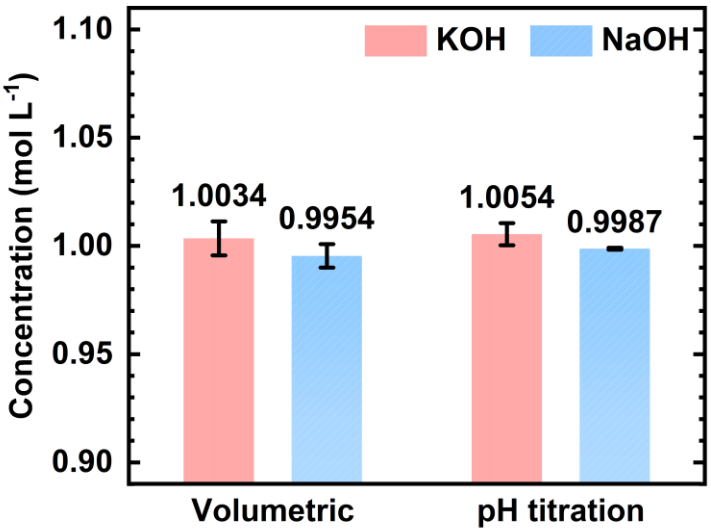

Figure S3. Molarities of KOH and NaOH electrolytes estimated from both volumetric and pH titration methods. Uncertainty bars represent standard deviations from six replicates.

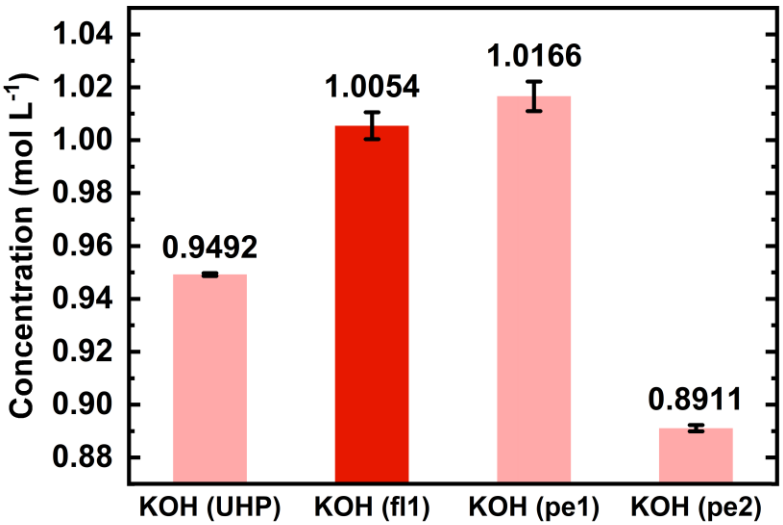

Figure S4. Molarities of different types and brands of KOH. The dark red bar highlights the KOH variety used throughout the rest of this study. UHP: ultra-high purity, fl: flake variety, pe: pellet variety. Numbers designate KOH manufacturers. Uncertainty bars represent standard deviations from six replicates.

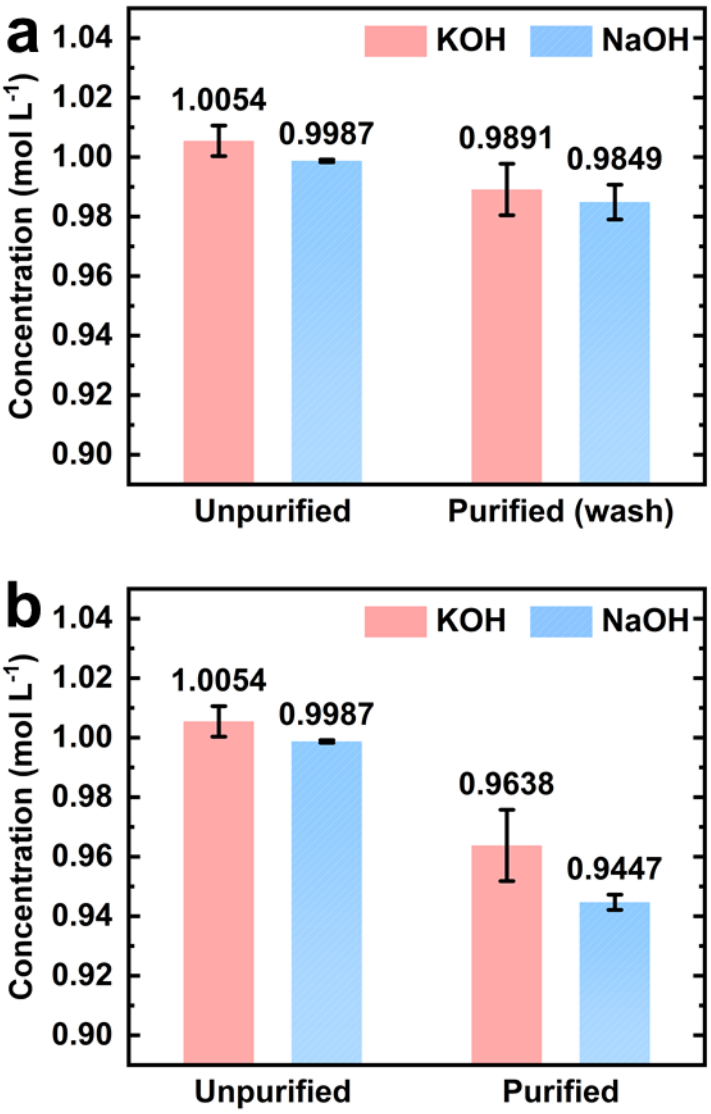

Figure S5. KOH electrolyte molarities before and after performing the proposed Fe removal routine: (a) when the $Ni(OH)_2$ precipitate is washed three times with 5 mL of fresh 1 M KOH and (b) without washing the precipitate. Uncertainty bars represent standard deviations from six replicates.

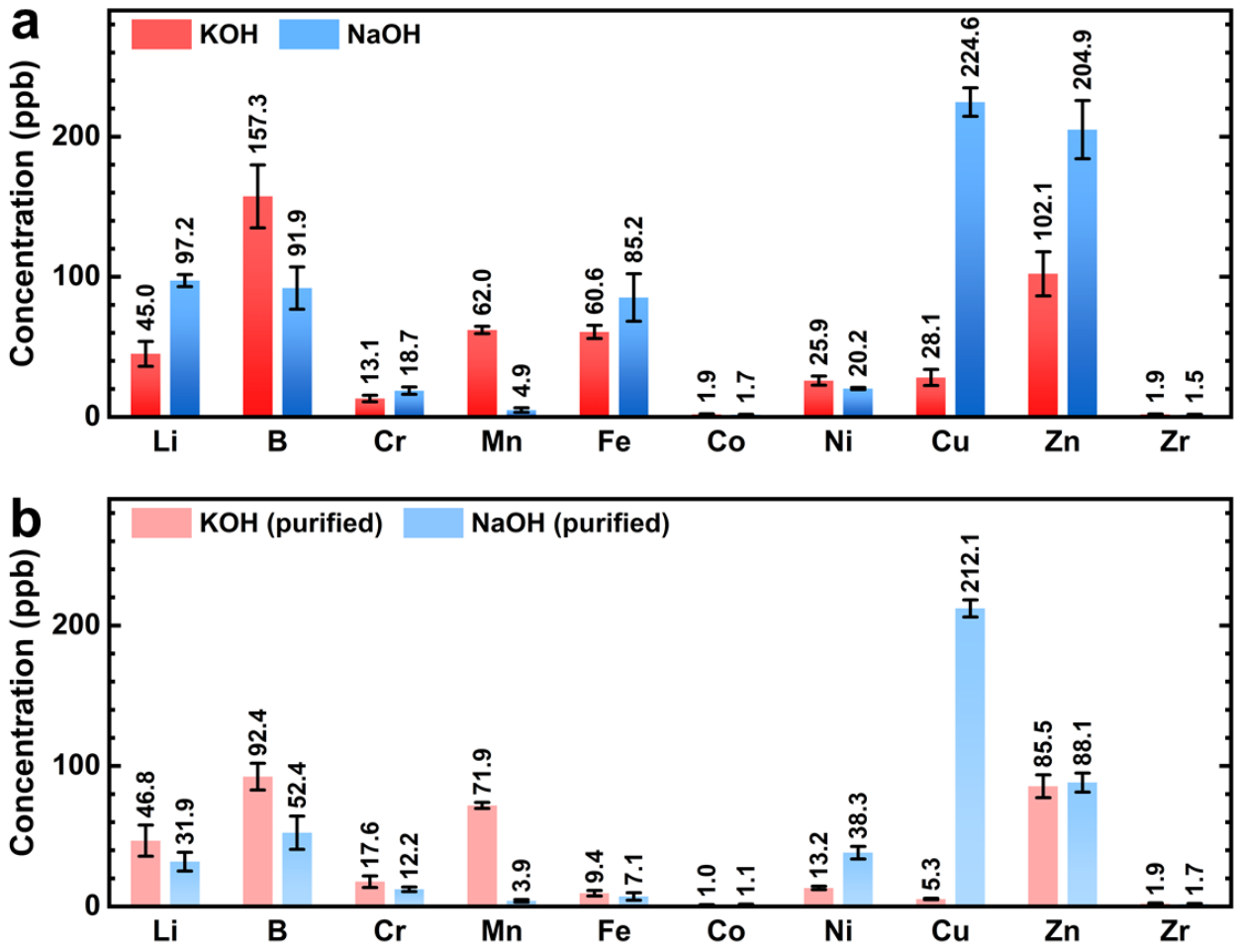

Figure S6. Complementary bar plots comparing the concentrations of primary elements in 1 M KOH and NaOH electrolytes: (a) unpurified and (b) purified electrolytes. Uncertainty bars represent standard deviations from five replicates.

Table S3. Detailed concentrations (in ppb) of primary elements in KOH and NaOH electrolytes from ICP-MS analysis

Unpurified KOH	^{7}Li	^{11}B	^{23}Na	^{24}Mg	^{28}Si	^{40}Ca	^{85}Rb	^{88}Sr	^{133}Cs	^{137}Ba	^{27}Al	^{52}Cr	^{55}Mn	^{56}Fe	^{59}Co	^{60}Ni	^{63}Cu	^{66}Zn	^{90}Zr	^{208}Pb
Mean	44.98	157.34	118384.02	276.82	267.39	5101.95	3403.94	10.77	1.86	104.08	488.32	13.09	62.03	60.62	1.87	25.91	28.13	102.07	1.88	1.94
SD	8.90	22.46	8497.96	42.22	53.59	742.27	276.49	0.71	0.23	12.46	71.05	2.30	2.64	4.72	0.31	3.25	5.77	15.76	0.19	0.36

Purified KOH	^{7}Li	^{11}B	^{23}Na	^{24}Mg	^{28}Si	^{40}Ca	^{85}Rb	^{88}Sr	^{133}Cs	^{137}Ba	^{27}Al	^{52}Cr	^{55}Mn	^{56}Fe	^{59}Co	^{60}Ni	^{63}Cu	^{66}Zn	^{90}Zr	^{208}Pb
Mean	46.81	92.41	116095.78	175.81	212.64	3085.52	3470.84	11.56	1.49	11.90	465.23	17.59	71.86	9.36	0.98	13.16	5.27	85.54	1.94	1.58
SD	11.06	9.54	458.10	38.42	25.96	619.40	15.53	1.94	0.29	2.45	56.18	4.14	2.16	1.99	0.29	1.20	0.55	8.11	0.47	0.29

Unpurified NaOH	^{7}Li	^{11}B	^{24}Mg	^{28}Si	^{39}K	^{40}Ca	^{85}Rb	^{88}Sr	^{133}Cs	^{137}Ba	^{27}Al	^{52}Cr	^{55}Mn	^{56}Fe	^{59}Co	^{60}Ni	^{63}Cu	^{66}Zn	^{90}Zr	^{208}Pb
Mean	97.24	91.91	187.4	385.75	15797.42	1657.36	6.47	25.11	1.31	75.22	818.56	18.72	4.92	85.17	1.67	20.22	224.58	204.93	1.54	2.16
SD	4.31	15.03	29.0	46.81	858.83	106.33	0.58	1.35	0.22	9.71	50.19	2.59	1.61	16.92	0.16	0.75	10.15	20.75	0.26	0.30

Purified NaOH	^{7}Li	^{11}B	^{24}Mg	^{28}Si	^{39}K	^{40}Ca	^{85}Rb	^{88}Sr	^{133}Cs	^{137}Ba	^{27}Al	^{52}Cr	^{55}Mn	^{56}Fe	^{59}Co	^{60}Ni	^{63}Cu	^{66}Zn	^{90}Zr	^{208}Pb
Mean	31.88	52.44	174.26	476.03	7089.55	1585.78	1.24	19.69	0.84	5.98	850.63	12.15	3.91	7.07	1.15	38.25	212.09	88.14	1.67	1.22
SD	6.67	11.86	23.80	116.67	930.98	136.67	0.15	1.68	0.29	1.36	40.86	1.61	0.94	2.63	0.50	4.50	6.12	6.80	0.37	0.21

UHP KOH	^{7}Li	^{11}B	^{23}Na	^{24}Mg	^{28}Si	^{40}Ca	^{85}Rb	^{88}Sr	^{133}Cs	^{137}Ba	^{27}Al	^{52}Cr	^{55}Mn	^{56}Fe	^{59}Co	^{60}Ni	^{63}Cu	^{66}Zn	^{90}Zr	^{208}Pb
Mean	78.77	ND	4617.43	76.33	145.63	342.22	198.87	3.95	2.15	24.36	56.41	18.40	64.71	17.68	0.43	5.48	10.27	62.63	3.04	ND
SD	8.13	ND	1538.90	4.97	45.88	46.67	2.19	0.55	0.34	5.35	12.74	3.51	5.77	4.34	0.09	0.43	1.78	16.33	0.68	ND

SD: standard deviation, ND: not detected/below detection limit

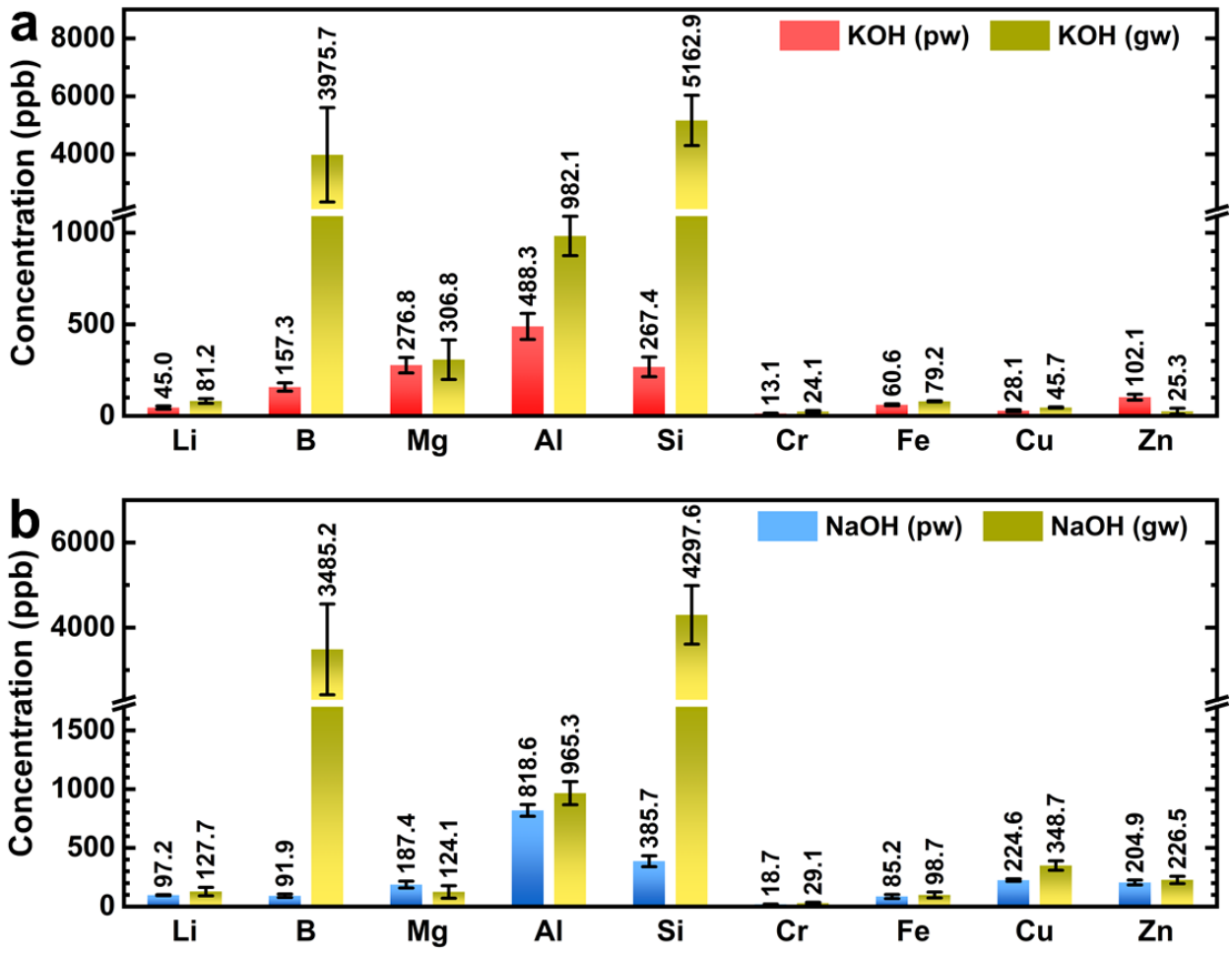

Figure S7. Comparison of critical elements varying their concentrations when using plasticware and glassware in unpurified (a) KOH and (b) NaOH electrolytes. Uncertainty bars represent standard deviations from three replicates. Note: pw – plasticware, gw – glassware.

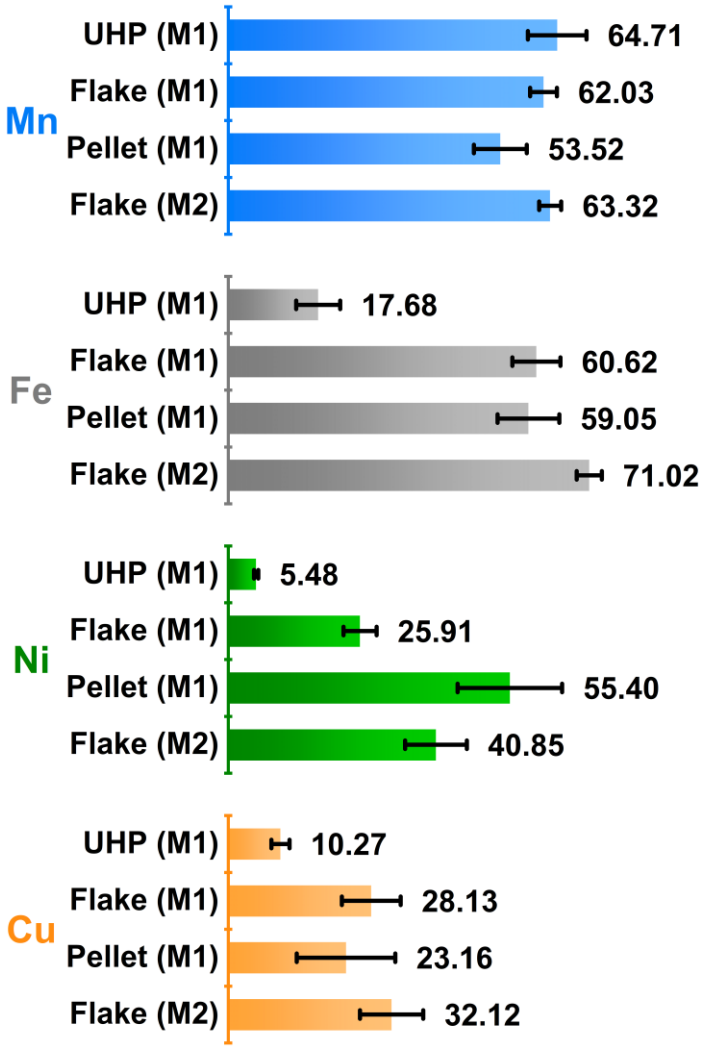

Figure S8. Mn, Fe, Ni, and Cu concentrations (in ppb) in unpurified KOH electrolytes prepared from different types of KOH. Numbers denote manufacturers. Uncertainty bars represent standard deviations from three replicates.

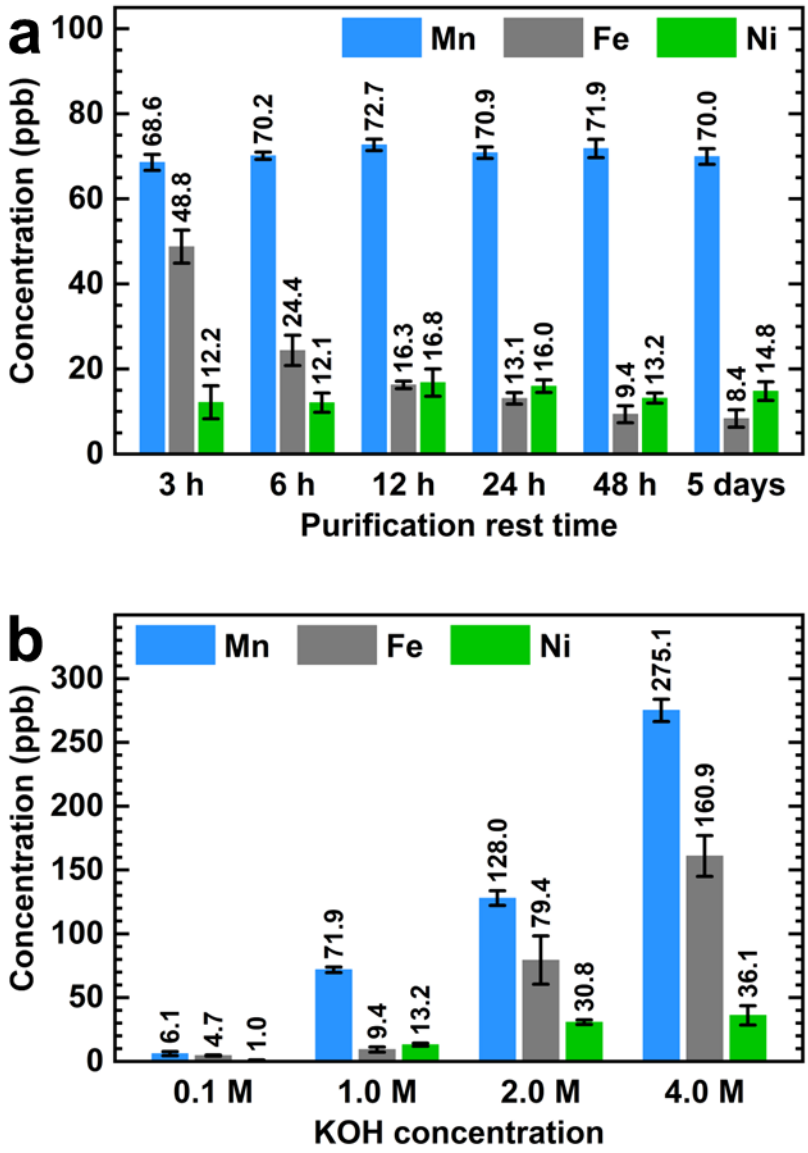

Figure S9. Effect of the experimental conditions on the proposed Fe purification routine: (a) purification rest time before the final centrifuge step, (b) concentration of KOH to be purified. Uncertainty bars represent standard deviations from three replicates.

Supporting Note 1: Coating the electrode is essential because it prevents the capillary action of the aqueous electrolyte.[35] Capillary action in porous electrodes increases the electrode surface wetted by the electrolyte, resulting in a surface area larger than the "immersed geometrical area," even when the "dry" area is flattened by metal clips. This effect is particularly negative when currents are normalized by the so-called "projected geometric area" because the wetted area may vary during measurements. Therefore, LSV scans recorded at different periods could exhibit larger current densities only because more surface area was exposed due to capillary action of the electrolyte. The capillary effect varies depending on the surface properties of the material, porosity, electrode dimensions, etc. Thus, the capillary effect results in fluctuating surface areas and low reproducibility, leading to unfair comparisons of electrocatalytic activity.[35] Consequently, the electrode surface area used to normalize the current should be carefully assessed when performing long-term stability and activation tests with porous electrodes.

Normalizing electrical currents using the electrochemical surface area (ECSA) is recommended whenever possible. However, estimating the ECSA involves several assumptions that could not apply to all the materials.[35–3737] As an alternative, coating the electrode with an inert material to keep the exposed geometrical area constant throughout the experiment can improve the reproducibility, at least when comparing the same substrate or during prolonged tests with the same electrode. Therefore, we used PDMS to limit the exposure of the Ni foam electrode to 1 cm^2 of projected geometrical area in all experiments. We highlight that we used the geometric area instead of the ECSA only because the PDMS coating enabled a reproducible immersed surface area, and the electrocatalyst and substrate were not changed.

Regarding the use of PDMS instead of other glues, such as epoxy resin,[7,35] we consider PDMS has more advantages for its use in aqueous media. PDMS is chemically inert (made only

of C, Si, O, and H), fully transparent, deformable, easy to mold, and highly hydrophobic. PDMS only suffers severe structural changes when immersed for more than 27 hours in KOH 87 wt.% at 55 ºC.[38] Importantly, PDMS remains liquid at room temperature for many hours before curing, and it becomes solid rapidly when proper heat treatment is applied (~10 min at 150 ºC).[39] From our experience, epoxy and other industrial glues are more viscous and require longer curing times. This results in poor infiltration into the porous matrix and leaves some inner pores exposed to capillary action. This is not the case for PDMS (see **Figure S2c**).

The main disadvantages of PDMS include the absorption of organic contaminants and swelling in hydrocarbon-based solvents,[39] which should not be an issue if used in high-purity aqueous electrolytes and if the PDMS-coated electrodes are washed with ethanol and acid before tests (like in any conventional Ni foam cleaning procedure). As shown in **Figure S10**, the electrolyte composition remains unchanged when the PDMS coating is used, confirming that PDMS does not release metal impurities that could affect the OER performance. Therefore, we recommend its use as a safe polymer coating to fix electrode geometric areas.

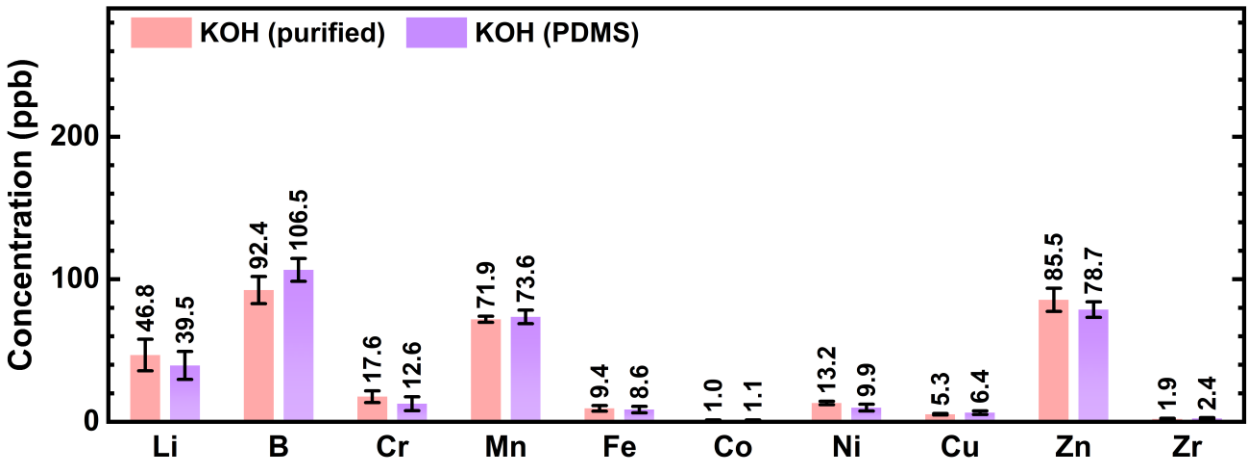

Figure S10. Comparison of main elements existing in purified KOH electrolyte before and after electrochemical tests using PDMS-coated Ni foam electrodes. Uncertainty bars represent standard deviations from three replicates.

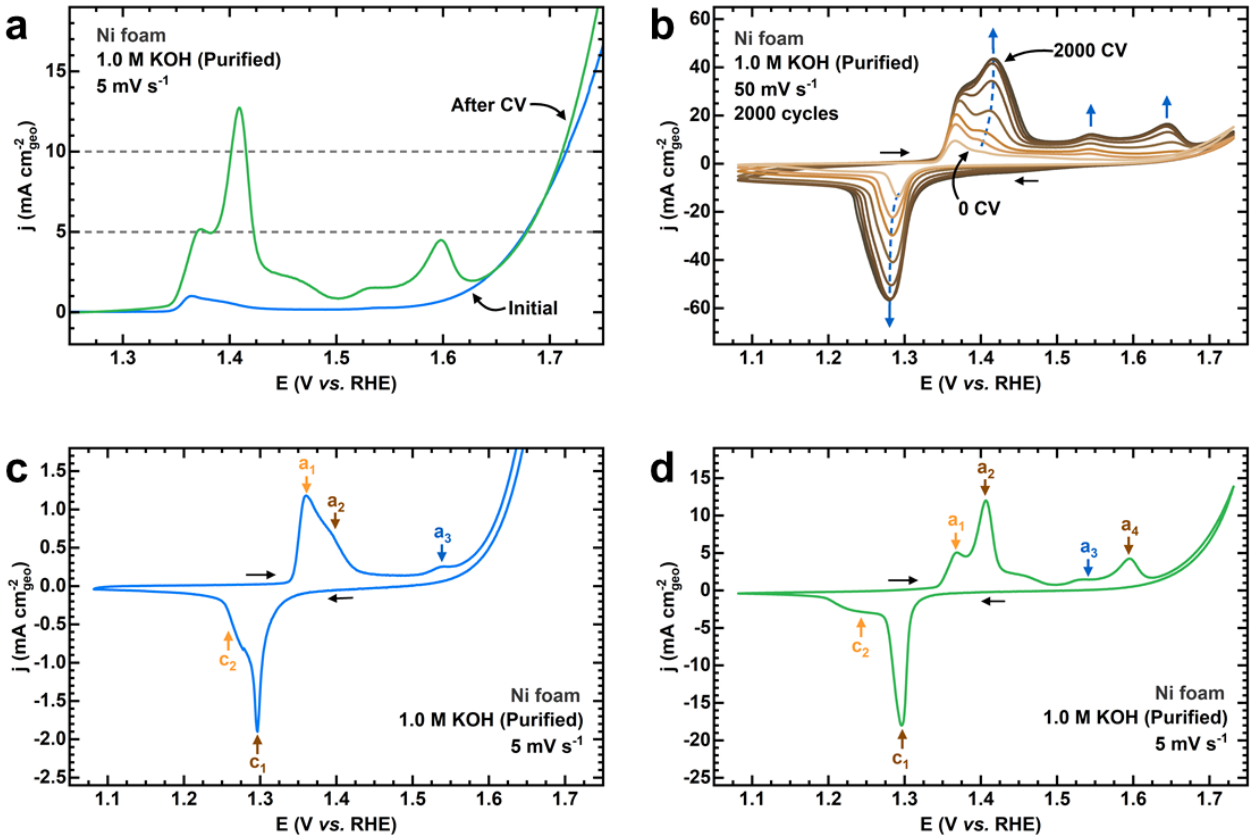

Figure S11. Electrochemical characterization of Ni foam electrodes in purified KOH: (a) anodic LSV scans before and after extended CV activation; (b) CV scans at different cycles during extended activation; CV scans at slow scan rate showing characteristic redox peaks (c) before and (d) after extended CV activation.

Supporting Note 2: Three prominent anodic peaks and two cathodic peaks can be seen in **Figure S11c**. Peaks $\mathbf{a_1}$ and $\mathbf{a_3}$ are attributed to the γ-NiOOH phase, where peak $\mathbf{a_1}$ indicates the oxidation of α-$Ni(OH)_2$ to γ-NiOOH and peak $\mathbf{a_3}$ can be attributed to the formation of Ni^{4+} species (likely NiO_2).[7,40] Moreover, peak $\mathbf{a_2}$ corresponds to the transformation of β-$Ni(OH)_2$ to β-NiOOH phase.[7,9] In the cathodic scan, peak $\mathbf{c_1}$ is attributed to the reduction of β-NiOOH to β-$Ni(OH)_2$,[7,9] whereas peak $\mathbf{c_2}$ corresponds to the reduction of γ-NiOOH to α-$Ni(OH)_2$.[40,41] The shape of the CV scan after extended CV activation changes significantly, as seen in **Figure S11d**. Peak $\mathbf{a_4}$ is now evident due to the decrease in OER current after aging and corresponds to β-NiOOH.[7,9] Furthermore, a decrease of the peak intensity of peaks $\mathbf{a_1}$ and $\mathbf{c_2}$ in contrast to the

increase of peaks **a**$_2$, **a**$_4$, and **c**$_1$ is indicative of the promotion of more ordered and compact β/β phase over the disordered α/γ phase during aging, which agrees with the Bode scheme shown in **Scheme 1**.[42] Note that the position of the peaks in **Figure S11d** agrees with the fact that the α/γ phase appears at more negative potentials than the β/β phase.[41–44]

Moreover, the increase in the intensity of peaks **a**$_3$ and **a**$_4$ after extended CV cycling (**Figures S11b** and **d**) is attributed to the overcharge of the β phase and transformation of β-NiOOH to γ-NiOOH when the upper potential limit lies beyond 0.7 V *vs.* Hg/HgO (~1.63 V *vs.* RHE).[7] Thus, it is evident that the Ni foam electrode activated after 2000 CV cycles is composed of a mixture of the α/γ and β/β phases, the latter being more predominant due to aging in Fe-purified 1 M KOH. In this study, we decided to scan the electrodes above 0.7 V *vs.* Hg/HgO to reach the 10 mA·cm^{-2} mark and monitor the overpotential decrease with cycling, causing the inevitable overcharge of the β phase to γ phase. We recommend performing CV scans with lower potential limits to reduce overcharge and promote the increase of peak **a**$_4$. Nevertheless, a mixture of both phases will inevitably be formed.[4,43]

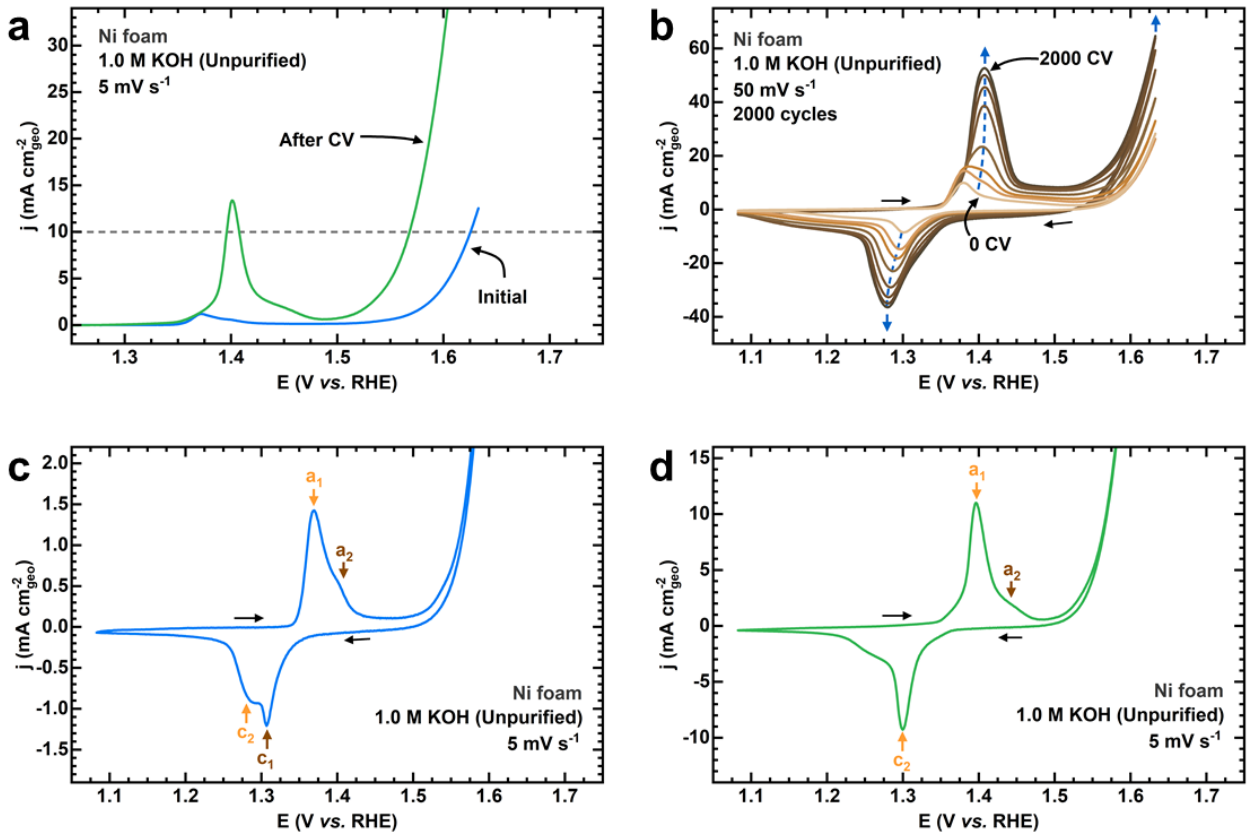

Figure S12. Electrochemical characterization of Ni foam electrodes in unpurified KOH: (a) anodic LSV scans before and after extended CV activation; (b) CV scans at different cycles during extended activation; CV scans at slow scan rate showing characteristic redox peaks (c) before and (d) after extended CV activation.

Supporting Note 3: In contrast to purified KOH (**Figure S11**), fewer peaks can be seen in the CV scans in unpurified KOH electrolyte. This is attributed to the increased disorder influenced by Fe incorporation into the layered structure.[4,7] According to Klaus *et al.*,[7] Fe incorporation inhibits the ordered β/β phase, and therefore the more disordered α/γ phase is preferentially formed during aging in unpurified KOH. The **a2** peak attributed to β-NiOOH is significantly smaller than the **a1** peak (γ-NiOOH phase) in **Figure S12c**. The anodic peak shifts to more positive potentials after extended cycling in unpurified 1 M KOH (**Figure S12d**), which is attributed to the ability of Fe to increase the oxidizing power of Ni^{2+}, making it more difficult to

be oxidized to $Ni^{3+/4+}$.[9,15,44,45] Note that the small shoulder at ~1.45 V *vs.* RHE could be attributed to a more repressed β/β phase, confirming the anodic shift of both Ni redox peaks.

In the cathodic scan, a sharp $\mathbf{c_2}$ peak shifts cathodically and obscures the $\mathbf{c_1}$ peak (**Figure S12b**). Thus, it is likely that it corresponds to α-$Ni(OH)_2$.[41] Nevertheless, the cathodic peak shift is not remarkable, and contrary to the anodic peak, it is hard to infer Fe incorporation just by looking at the cathodic peak. Furthermore, the significant increase of the OER activity by lowering the overpotential obscures the $\mathbf{a_3}$ and $\mathbf{a_4}$ peaks from **Figure S11d**. The disappearance of these peaks can be regarded as a definitive criterion of Fe impurities, confirming the Fe incorporation into Ni foam electrodes aged in unpurified 1 M KOH (~60 ppb Fe).

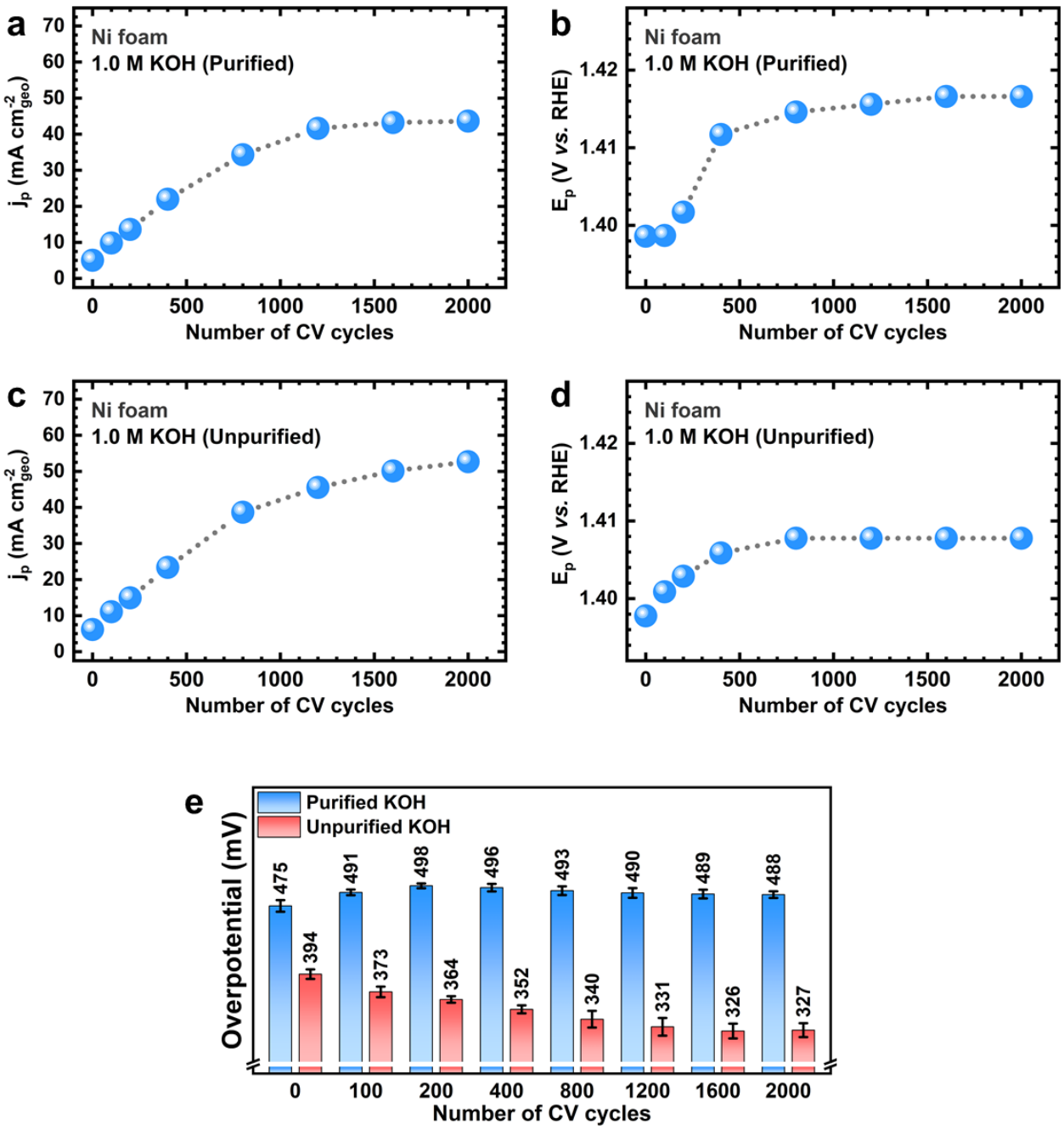

Figure S13. Parameters varying during extended CV activation of Ni foam electrodes in KOH electrolytes: changes in the (a) peak current and (b) peak potential of *β*/*β* redox peak (dashed arrow from **Figure S11b**) of Ni foam in purified KOH; changes in the (c) peak current and (d) peak potential of the *α*/*γ* redox peak (dashed arrow from **Figure S12b**) of Ni foam in unpurified KOH; (e) overpotentials at 10 mA cm^{-2} at different cycle number during extended CV activation.

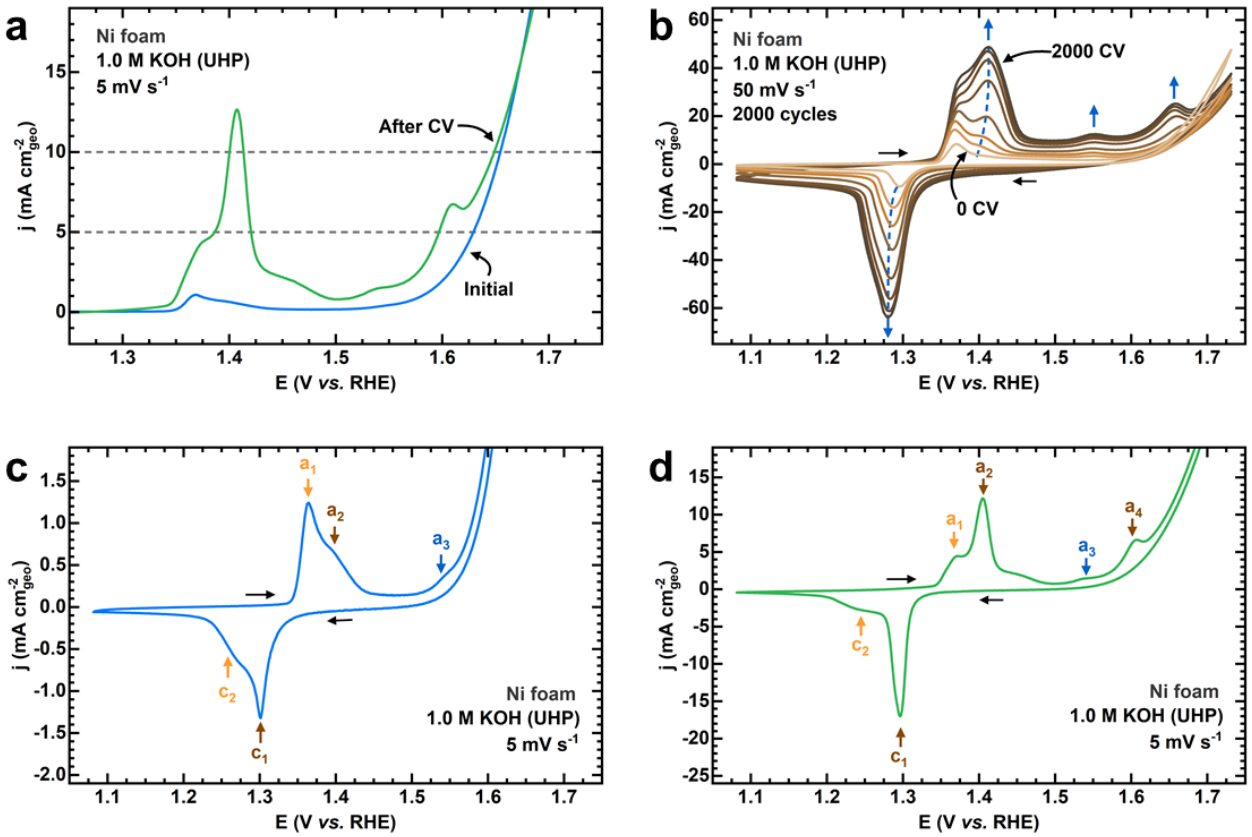

Figure S14. Electrochemical characterization of Ni foam electrodes in ultra-high purity KOH: (a) anodic LSV scans before and after extended CV activation; (b) CV scans at different cycles during extended activation; CV scans at slow scan rate showing characteristic redox peaks (c) before and (d) after extended CV activation.

Supporting Note 4: As shown in **Figure S13e**, the Ni foam sample activated in purified KOH electrolyte exhibited a significant overpotential increase until ~200 cycles. This is the expected behavior, as experimental evidence suggests that the *β*/*β* phase is a poor OER electrocatalyst, and the OER overpotential should increase upon aging.[7,9] However, we found that further cycling results in an apparent "decrease" of the overpotential (488 mV at 2000 cycles) that differs ~10 mV from the highest overpotential (498 mV at 200 cycles). Statistically speaking, the uncertainty from our replicates confirms that there is no significant difference among overpotentials after 800 cycles, suggesting that there is no meaningful decrease of the overpotential after activation in purified 1 M KOH (~9 ppb Fe).

However, we noted a subtle decrease in the overpotential in UHP 1 M KOH. As shown in **Figure S14b**, the overpotential drastically increased in the initial 500 cycles and then decreased again. LSV scans in **Figure S14a** show a significant decrease of the OER overpotential after activation instead of the expected increase and stabilization in purified 1 M KOH (~9 ppb Fe). We extended the aging process by performing an additional set of 2000 CV cycles using the same Ni foam electrode but adding fresh UHP 1 M KOH electrolyte (**Figure S15**). LSV scans in **Figure S15a** revealed a slight decrease in the overpotential after activation. Moreover, the OER overpotentials remained relatively constant (*i.e.*, there was no further increase of the overpotential as expected) during activation, as revealed by the CV scans in **Figure S15b**.

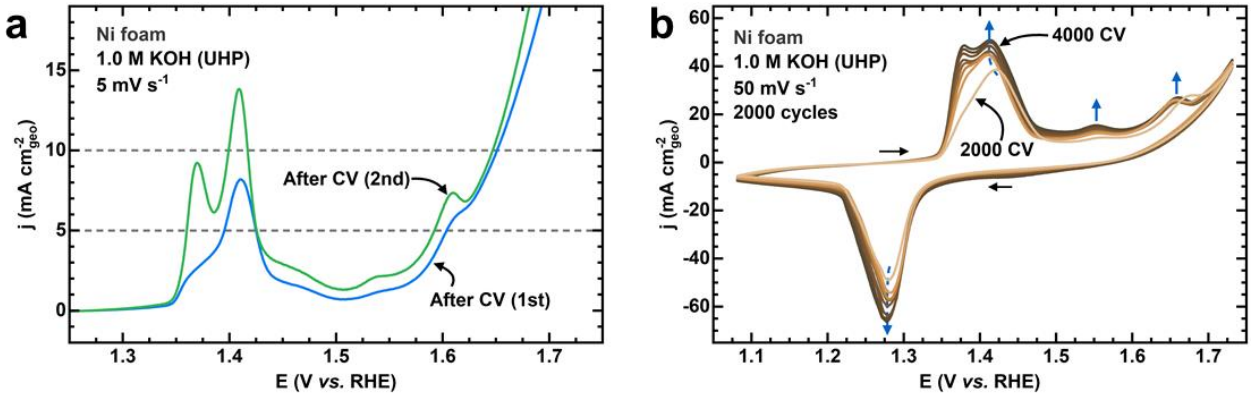

Figure S15. Electrochemical characterization of Ni foam electrodes in ultra-high purity KOH in the second set of 2000 cycles: (a) anodic LSV scans before and after extended CV activation; (b) CV scans at different cycles during extended activation.

We postulate two main theories regarding this interesting behavior. First, note that the concentration of Fe in UHP 1 M KOH is ~18 ppb, which doubles the concentration in the KOH purified through our routine and is roughly three times lower than the concentration in unpurified KOH (~60 ppb). Our experimental evidence suggests that even with such low levels of Fe, the electrodes still incorporate small amounts of Fe that remain undetectable from analytical techniques with low sensitivity (we could not detect Fe using EDX on the surface of these

electrodes, and previous studies from our group have not detected Fe using XPS). These subtle effects could only be detected after prolonged electrochemical aging, although there is no significant improvement in the OER activity.

Second, we used Ni foam electrodes with a large surface area and a small electrolyte volume of ~30 mL, maximizing the contact with the electrolyte, and therefore, the Fe uptake could have increased during long-term activation. Overall, these experiments demonstrate that (a) even small traces of Fe (in the order of 20 ppb) could indeed cause fluctuations in OER overpotentials after long-term exposure and that (b) it is almost impossible to avoid Fe incorporation. Nevertheless, we encourage future studies to examine Fe incorporation to determine if Fe impurities are responsible for any significant change in the OER overpotential. Fe incorporation could be negligible only if overpotential differences are not statistically significant.

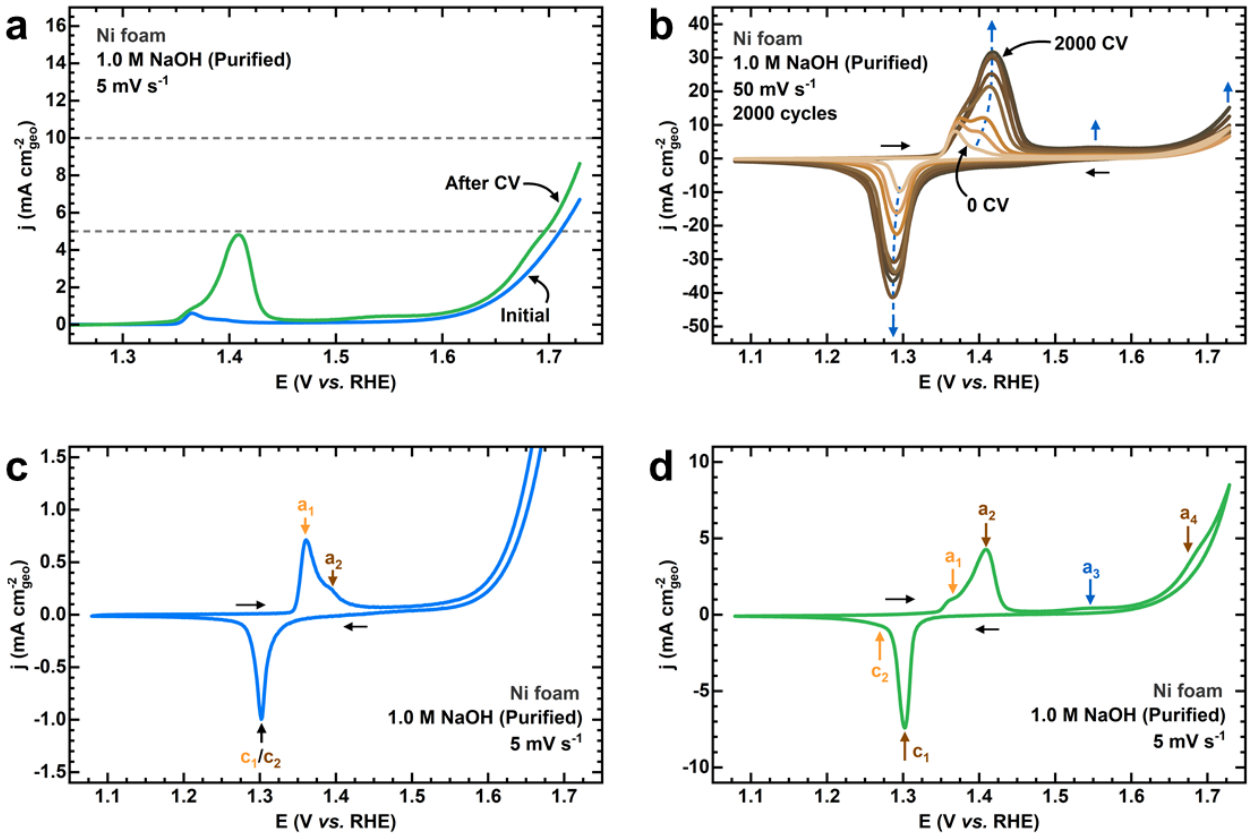

Figure S16. Electrochemical characterization of Ni foam electrodes in purified NaOH: (a) anodic LSV scans before and after extended CV activation; (b) CV scans at different cycles during extended activation; CV scans at slow scan rate showing characteristic redox peaks (c) before and (d) after extended CV activation.

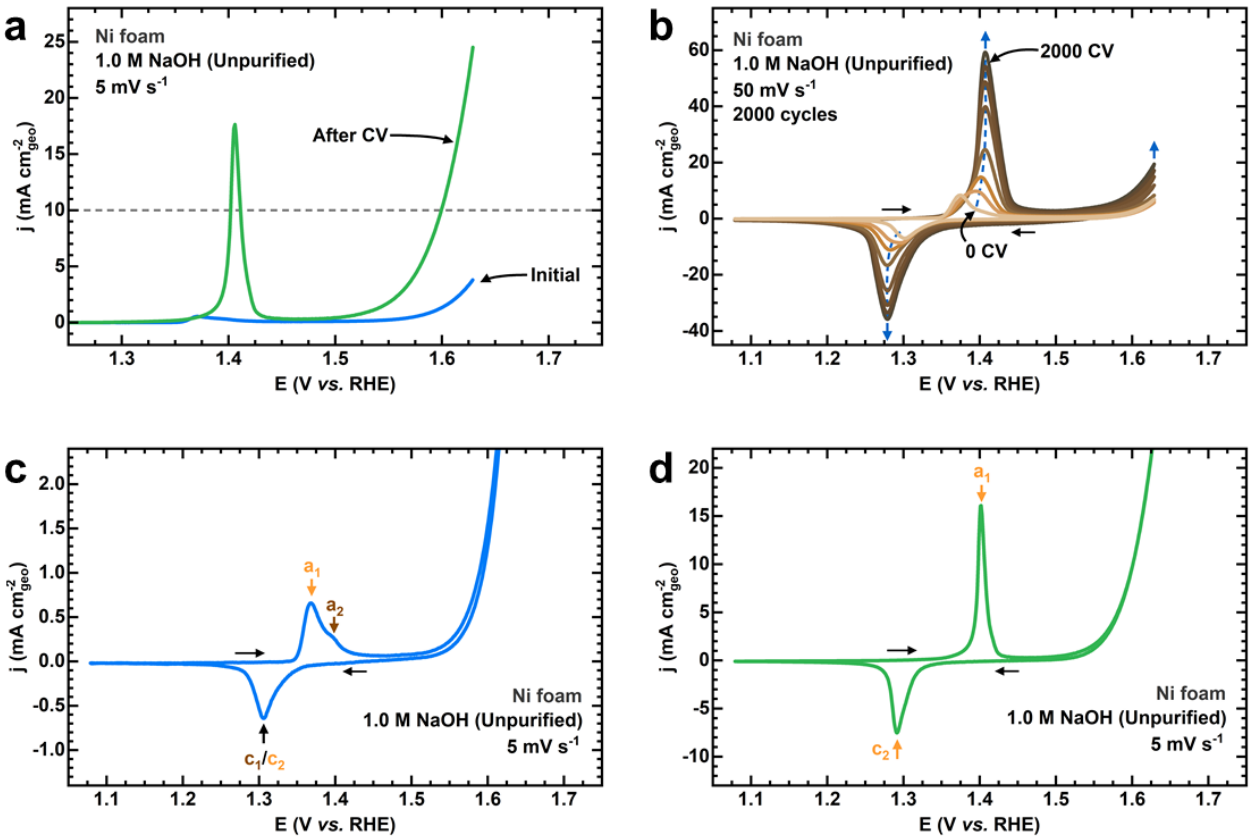

Figure S17. Electrochemical characterization of Ni foam electrodes in unpurified NaOH: (a) anodic LSV scans before and after extended CV activation; (b) CV scans at different cycles during extended activation; CV scans at slow scan rate showing characteristic redox peaks (c) before and (d) after extended CV activation.

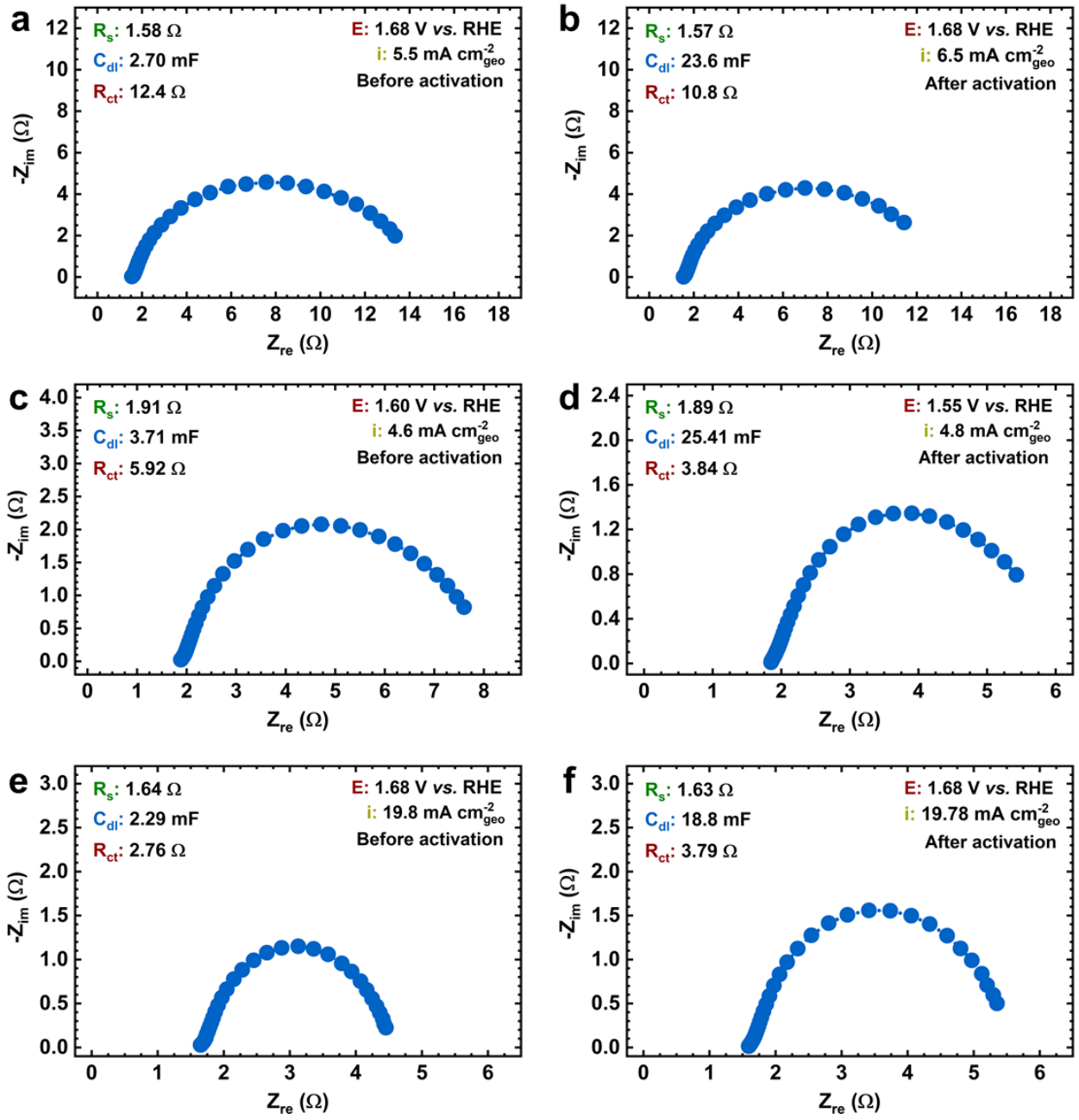

Figure S18. EIS measurements of Ni foam electrodes in KOH electrolyte before (left column) and after (right column) extended CV activation: purified (a, b), unpurified (c, d), and ultra-high purity (e, f).

Table S4. EIS parameters of Ni foam electrodes before and after extended CV activation in KOH electrolytes

Electrolyte	$E_{Hg/HgO}$ (V)	E_{RHE} (V)	j (mA cm^{-2})	R_u (Ω)	C_{dl} (mF)	ω_{max} (Hz)	R_{ct} (Ω)
Unpurified KOH (Before)	0.67	1.603	4.57	1.91	3.71	7.92	5.92
Unpurified KOH (After)	0.67	1.603	32.02	1.88	14.55	9.95	1.15
Unpurified KOH (After)	0.62	1.553	4.80	1.89	25.41	1.57	3.84
Fe-free KOH (Before)	0.75	1.683	5.48	1.58	2.70	4.99	12.37
Fe-free KOH (After)	0.75	1.683	6.52	1.57	23.60	0.64	10.76
Fe-free KOH (After)	0.74	1.675	5.47	1.57	23.91	0.45	15.13
UHP KOH (Before)	0.75	1.683	19.78	1.64	2.29	24.86	2.76
UHP KOH (After)	0.75	1.683	19.78	1.63	18.80	2.45	3.79
UHP KOH (After)	0.75	1.683	19.78	1.64	18.34	2.24	4.01

Supporting Note 5: EIS fitting of the curves shown in **Figure S18** was done using the general Randles equivalent circuit model, modeling the C_{dl} with a constant-phase element, the charge transfer resistance (R_{ct}) with a resistor in parallel to the C_{dl}, and R_u as the solution resistance in series.[46] We also fitted EIS data using two additional models proposed in the literature, (1) the Armstrong-Henderson equivalent circuit for modeling OER catalysts,[14,47–50] and (2) the Bisquert open transmission line model for porous electrodes.[15] We note, however, that the additional resistance terms (R_{ads} for the OER model and R_m film resistance for the Bisquert open model) were significantly smaller than the R_{ct} term and considered as negligible (even the Randles circuit resulted in better goodness of fit and residuals close to zero). Similarly, the rest of the parameters (R_u and C_{dl}) did not change among the models. Thus, we used the general Randles model only for comparison purposes. However, we encourage researchers to use appropriate equivalent models suitable to each electrocatalytic material.

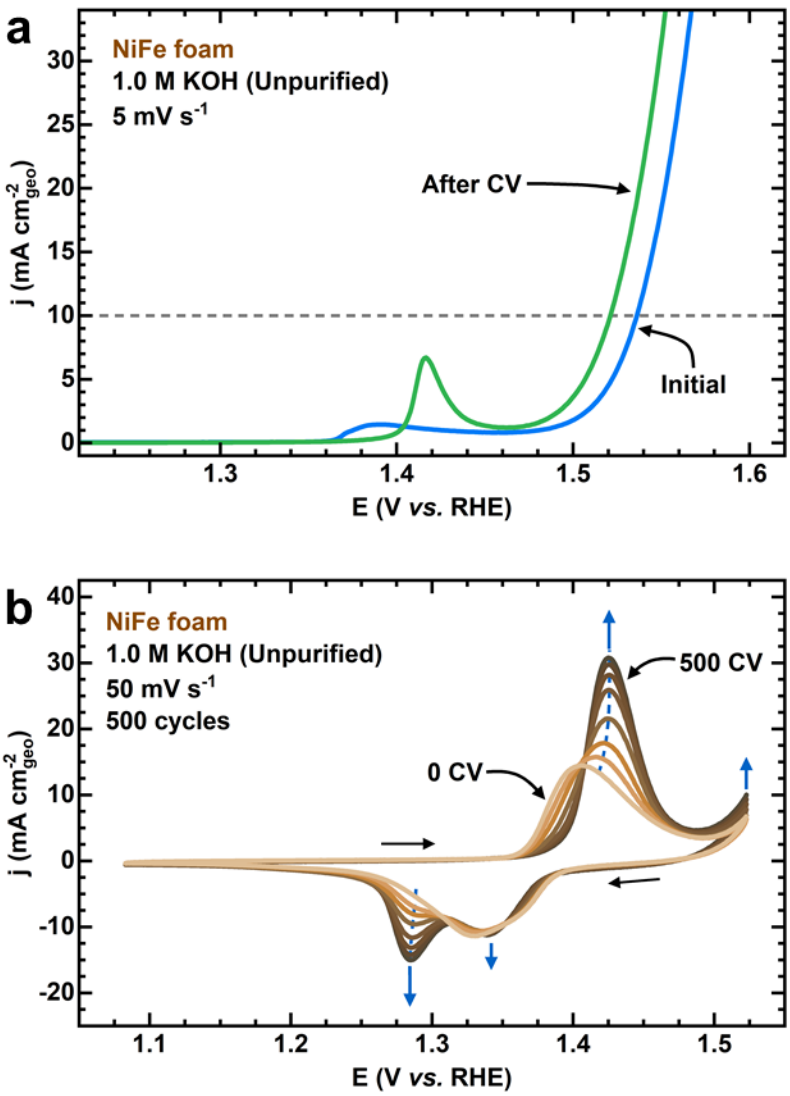

Figure S19. Electrochemical characterization of a NiFe foam electrode in unpurified KOH: (a) anodic LSV scans before and after extended CV activation; (b) CV scans at different cycles during extended activation.

Supporting Note 6: LSV curves before and after activation of NiFe foam in unpurified KOH (**Figure S19a**) show an increase of the OER activity (~15 mV overpotential decrease). Moreover, CV scans in **Figure S19b** suggest that activation of the NiFe foam electrode promotes the formation of the α/γ phase (cathodic and anodic peaks increase), followed by a slight increase in the OER current. Although the increase in the intensity of the redox peaks could be attributed to the disordering of the Ni phase during activation, the increase of OER activity suggests Fe

incorporation from the electrolyte. EDX measurements of the NiFe electrode before and after activation confirm the incorporation of more Fe (**Figure S20**). Furthermore, EIS measurements (**Figure S21** and **Table S5**) show that (1) the C_{dl} almost doubles after activation and (2) the R_{ct} slightly decreases when compared at the same potential and increases when compared at the same current density. Therefore, the experimental evidence suggests that Ni-based materials with some initial percent of Fe can still incorporate more Fe from unpurified electrolytes and increase their OER activity further.

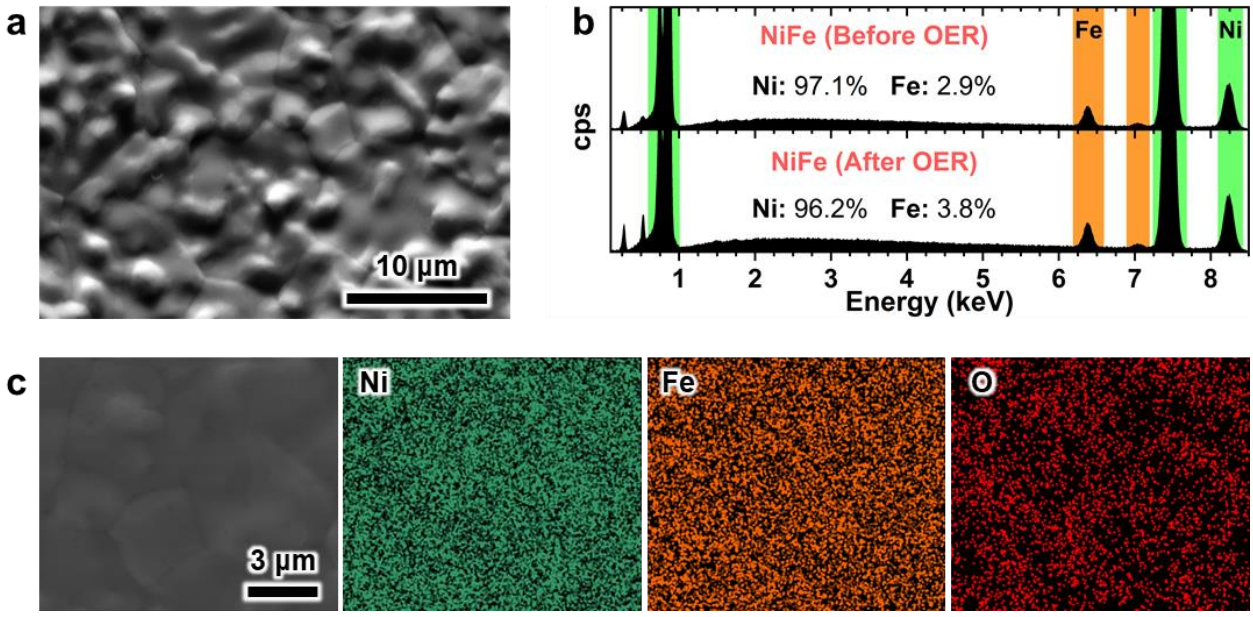

Figure S20. Physicochemical characterization of the NiFe foam electrode: (a) SEM image of the pristine NiFe foam surface, (b) EDX spectra and Ni:Fe compositions before and after CV activation, (c) EDX elemental mappings of the NiFe foam surface.

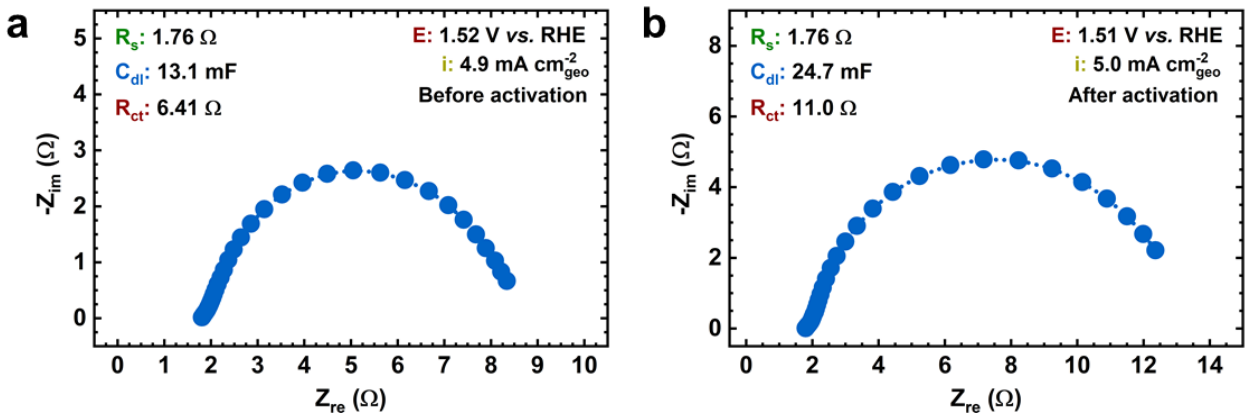

Figure S21. EIS measurements of the NiFe foam electrode in unpurified KOH electrolyte (a) before and (b) after CV activation.

Table S5. EIS parameters of the NiFe foam electrode before and after CV activation in unpurified KOH electrolyte

Electrolyte	$E_{Hg/HgO}$ (V)	E_{RHE} (V)	j (mA cm^{-2})	R_u (Ω)	C_{dl} (mF)	ω_{max} (Hz)	R_{ct} (Ω)
Unpurified KOH (Before)	0.59	1.523	4.89	1.76	13.11	1.98	6.41
Unpurified KOH (After)	0.59	1.523	10.39	1.75	22.21	1.99	3.50
Unpurified KOH (After)	0.58	1.508	5.02	1.76	24.69	0.64	11.03

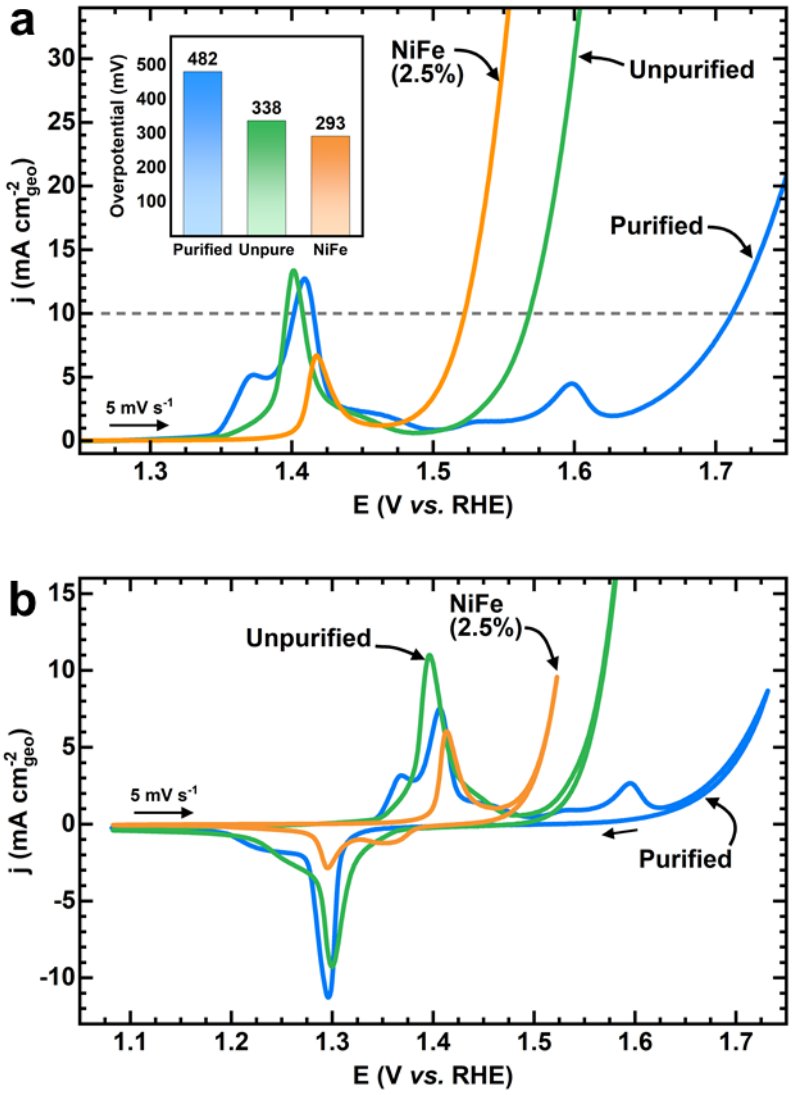

Figure S22. Comparison of the effect of Fe impurities in Ni foam (purified, unpurified) and NiFe foam (unpurified) electrodes in KOH electrolytes: (a) anodic LSV scans after extended CV activation; (b) CV scans at slow scan rate showing characteristic redox peaks.

Supporting Note 7: Figure S22 demonstrates how Fe incorporation decreases the OER overpotential and shifts the $Ni^{2+/3+}$ peaks anodically. From **Figure S22a**, the Ni foam electrode in Fe-purified KOH shows prominent redox peaks for the *β*/*β* phase (at ~1.4 *vs.* RHE) and the *β* to *γ* phase transition due to overcharge (at ~1.55 and ~1.6 V *vs.* RHE), a small peak for the *α*/*γ* phase (at ~1.36 V *vs.* RHE) and the highest overpotential at 10 mA·cm^{-2} (inset, 482 mV). In unpurified

KOH electrolyte, the anodic peak attributed to the α/γ phase shifts to ~1.4 V *vs.* RHE, almost overlapping with the peak for the β/β phase in Fe-purified electrolyte, and the OER overpotential decreases to 338 mV, obscuring the redox peaks for the β to γ phase transition. Finally, the NiFe foam electrode exhibits the most significant peak shift to ~1.42 V *vs.* RHE and results in the lowest OER overpotential (293 mV). CVs in **Figure S22b** display the same trends for anodic peak shifts and OER potentials after activation. Note, however, that the cathodic peak position does not change significantly. Hence, we advocate that tracking anodic peak positions and OER overpotentials during electrode activation can be effectively used to determine if some degree of Fe incorporation occurs.

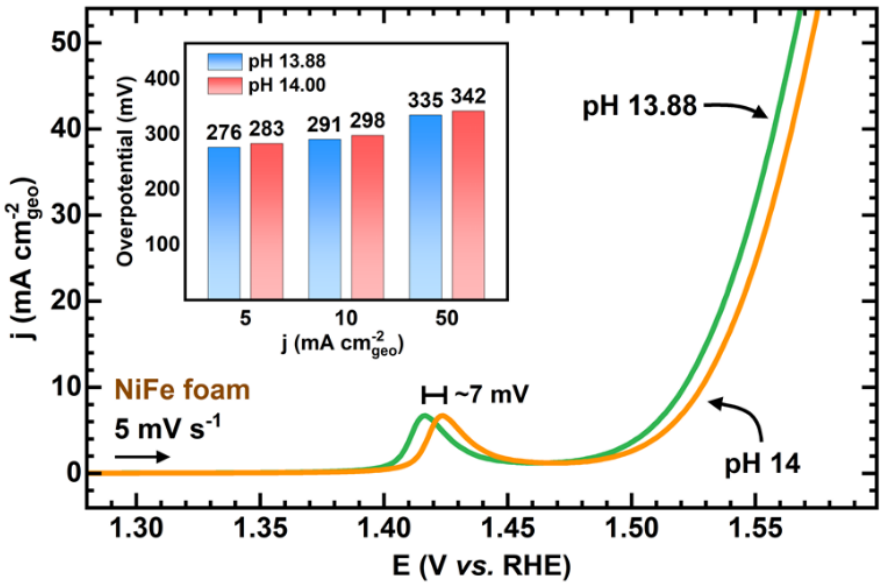

Figure S23. LSV scans of a NiFe foam electrode in 1 M KOH after CV activation (500 cycles). The potential shift caused by assuming a pH of 14 in the RHE conversion equation is shown. Inset: overpotentials at 5, 10, and 50 mA cm^{-2}.

Supporting Note 8: *why do we need to care about accurate potential conversion?* **Figure S23** shows a potential shift of just 7 mV (predicted theoretically by the Nernst equation) resulting from the common assumption of pH 14 for 1 M alkaline electrolytes.[3,44,51] We note that this "slight" deviation can result in wrong estimations of OER overpotentials and redox peak positions. For instance, one could incorrectly infer the presence of impurities if the redox peak at pH 14 does not match the one from previous publications. Thus, incorrect estimation of electrode potentials results in erroneous descriptions and unfair comparisons of electrochemical performance metrics. Therefore, future studies should not consider the electrolyte's properties as "trivial," and precise descriptions of electrolyte concentration and composition should always be provided.

References

(1) Christian, G. D.; Dasgupta, P. K.; Schug, K. A. *Analytical Chemistry*, Seventh Edition.; John Wiley & Sons, 2014.

(2) Harris, D. C.; Lucy, C. A. *Quantitative Chemical Analysis*, Ninth Edition.; W. H. Freeman and Company, 2016.

(3) Hausmann, J. N.; Traynor, B.; Myers, R. J.; Driess, M.; Menezes, P. W. The PH of Aqueous NaOH/KOH Solutions: A Critical and Non-Trivial Parameter for Electrocatalysis. *ACS Energy Lett.* **2021**, 3567–3571. https://doi.org/10.1021/acsenergylett.1c01693.

(4) Louie, M. W.; Bell, A. T. An Investigation of Thin-Film Ni–Fe Oxide Catalysts for the Electrochemical Evolution of Oxygen. *J. Am. Chem. Soc.* **2013**, *135* (33), 12329–12337. https://doi.org/10.1021/ja405351s.

(5) Garcia, A. C.; Koper, M. T. M. Effect of Saturating the Electrolyte with Oxygen on the Activity for the Oxygen Evolution Reaction. *ACS Catal.* **2018**, *8* (10), 9359–9363. https://doi.org/10.1021/acscatal.8b01447.

(6) Spendelow, J. S.; Goodpaster, J. D.; Kenis, P. J. A.; Wieckowski, A. Mechanism of CO Oxidation on Pt(111) in Alkaline Media. *J. Phys. Chem. B* **2006**, *110* (19), 9545–9555. https://doi.org/10.1021/jp060100c.

(7) Klaus, S.; Cai, Y.; Louie, M. W.; Trotochaud, L.; Bell, A. T. Effects of Fe Electrolyte Impurities on Ni(OH)2/NiOOH Structure and Oxygen Evolution Activity. *J. Phys. Chem. C* **2015**, *119* (13), 7243–7254. https://doi.org/10.1021/acs.jpcc.5b00105.

(8) Trześniewski, B. J.; Diaz-Morales, O.; Vermaas, D. A.; Longo, A.; Bras, W.; Koper, M. T. M.; Smith, W. A. In Situ Observation of Active Oxygen Species in Fe-Containing Ni-Based Oxygen Evolution Catalysts: The Effect of PH on Electrochemical Activity. *J. Am. Chem. Soc.* **2015**, *137* (48), 15112–15121. https://doi.org/10.1021/jacs.5b06814.

(9) Trotochaud, L.; Young, S. L.; Ranney, J. K.; Boettcher, S. W. Nickel–Iron Oxyhydroxide Oxygen-Evolution Electrocatalysts: The Role of Intentional and Incidental Iron Incorporation. *J. Am. Chem. Soc.* **2014**, *136* (18), 6744–6753. https://doi.org/10.1021/ja502379c.

(10) Subbaraman, R.; Danilovic, N.; Lopes, P. P.; Tripkovic, D.; Strmcnik, D.; Stamenkovic, V. R.; Markovic, N. M. Origin of Anomalous Activities for Electrocatalysts in Alkaline Electrolytes. *J. Phys. Chem. C* **2012**, *116* (42), 22231–22237. https://doi.org/10.1021/jp3075783.

(11) Trotochaud, L.; Ranney, J. K.; Williams, K. N.; Boettcher, S. W. Solution-Cast Metal Oxide Thin Film Electrocatalysts for Oxygen Evolution. *J. Am. Chem. Soc.* **2012**, *134* (41), 17253–17261. https://doi.org/10.1021/ja307507a.

(12) Conway, B. E.; Bourgault, P. L. Significance of e.m.f. Decay Measurements. Applications to the Nickel Oxide Electrode. *Trans. Faraday Soc.* **1962**, *58* (0), 593–607. https://doi.org/10.1039/TF9625800593.

(13) Chung, D. Y.; Lopes, P. P.; Farinazzo Bergamo Dias Martins, P.; He, H.; Kawaguchi, T.; Zapol, P.; You, H.; Tripkovic, D.; Strmcnik, D.; Zhu, Y.; Seifert, S.; Lee, S.; Stamenkovic, V. R.; Markovic, N. M. Dynamic Stability of Active Sites in Hydr(Oxy)Oxides for the Oxygen Evolution Reaction. *Nat. Energy* **2020**, *5* (3), 222–230. https://doi.org/10.1038/s41560-020-0576-y.

(14) Swierk, J. R.; Klaus, S.; Trotochaud, L.; Bell, A. T.; Tilley, T. D. Electrochemical Study of the Energetics of the Oxygen Evolution Reaction at Nickel Iron (Oxy)Hydroxide Catalysts. *J. Phys. Chem. C* **2015**, *119* (33), 19022–19029. https://doi.org/10.1021/acs.jpcc.5b05861.

(15) Son, Y. J.; Kawashima, K.; Wygant, B. R.; Lam, C. H.; Burrow, J. N.; Celio, H.; Dolocan, A.; Ekerdt, J. G.; Mullins, C. B. Anodized Nickel Foam for Oxygen Evolution Reaction in Fe-Free and Unpurified Alkaline Electrolytes at High Current Densities. *ACS Nano* **2021**, *15* (2), 3468–3480. https://doi.org/10.1021/acsnano.0c10788.

(16) Liu, L.; Twight, L. P.; Fehrs, J. L.; Ou, Y.; Sun, D.; Boettcher, S. W. Purification of Residual Ni and Co Hydroxides from Fe-Free Alkaline Electrolyte for Electrocatalysis Studies. *ChemElectroChem* **2022**, *9* (15), e202200279. https://doi.org/10.1002/celc.202200279.

(17) Patidar, R.; Rebary, B.; Bhadu, G. R.; Patel, G. ICP-MS Method Development and Validation for Determination of Trace Elemental Impurities in Caustic Potash. *International Journal of Mass Spectrometry* **2020**, *454*, 116356. https://doi.org/10.1016/j.ijms.2020.116356.

(18) Lu, Y.; Sun, Y. An On-Line Electrodialyzer-ICP-MS Analytical System for Direct Determination of Trace Metal Impurities in KOH. *J. Anal. At. Spectrom.* **2008**, *23* (4), 574–578. https://doi.org/10.1039/B712296A.

(19) Márquez, R. A.; Kawashima, K.; Son, Y. J.; Rose, R.; Smith, L. A.; Miller, N.; Carrasco Jaim, O. A.; Celio, H.; Mullins, C. B. Tailoring 3D-Printed Electrodes for Enhanced Water Splitting. *ACS Appl. Mater. Interfaces* **2022**, *14* (37), 42153–42170. https://doi.org/10.1021/acsami.2c12579.

(20) Jovanovič, P.; Hodnik, N.; Ruiz-Zepeda, F.; Arčon, I.; Jozinović, B.; Zorko, M.; Bele, M.; Šala, M.; Šelih, V. S.; Hočevar, S.; Gaberščček, M. Electrochemical Dissolution of Iridium and Iridium Oxide Particles in Acidic Media: Transmission Electron Microscopy, Electrochemical Flow Cell Coupled to Inductively Coupled Plasma Mass Spectrometry, and X-Ray Absorption Spectroscopy Study. *J. Am. Chem. Soc.* **2017**, *139* (36), 12837–12846. https://doi.org/10.1021/jacs.7b08071.

(21) Kasian, O.; Geiger, S.; Li, T.; Grote, J.-P.; Schweinar, K.; Zhang, S.; Scheu, C.; Raabe, D.; Cherevko, S.; Gault, B.; Mayrhofer, K. J. J. Degradation of Iridium Oxides via Oxygen Evolution from the Lattice: Correlating Atomic Scale Structure with Reaction Mechanisms. *Energy Environ. Sci.* **2019**, *12* (12), 3548–3555. https://doi.org/10.1039/C9EE01872G.

(22) Cherevko, S.; Zeradjanin, A. R.; Topalov, A. A.; Kulyk, N.; Katsounaros, I.; Mayrhofer, K. J. J. Dissolution of Noble Metals during Oxygen Evolution in Acidic Media. *ChemCatChem* **2014**, *6* (8), 2219–2223. https://doi.org/10.1002/cctc.201402194.

(23) Gatalo, M.; Jovanovič, P.; Polymeros, G.; Grote, J.-P.; Pavlišič, A.; Ruiz- Zepeda, F.; Šelih, V. S.; Šala, M.; Hočevar, S.; Bele, M.; Mayrhofer, K. J. J.; Hodnik, N.; Gaberščček, M. Positive Effect of Surface Doping with Au on the Stability of Pt-Based Electrocatalysts. *ACS Catal.* **2016**, *6* (3), 1630–1634. https://doi.org/10.1021/acscatal.5b02883.

(24) Geiger, S.; Kasian, O.; Ledendecker, M.; Pizzutilo, E.; Mingers, A. M.; Fu, W. T.; Diaz-Morales, O.; Li, Z.; Oellers, T.; Fruchter, L.; Ludwig, A.; Mayrhofer, K. J. J.; Koper, M. T. M.; Cherevko, S. The Stability Number as a Metric for Electrocatalyst Stability Benchmarking. *Nat Catal* **2018**, *1* (7), 508–515. https://doi.org/10.1038/s41929-018-0085-6.

(25) Frydendal, R.; Paoli, E. A.; Knudsen, B. P.; Wickman, B.; Malacrida, P.; Stephens, I. E. L.; Chorkendorff, I. Benchmarking the Stability of Oxygen Evolution Reaction Catalysts: The Importance of Monitoring Mass Losses. *ChemElectroChem* **2014**, *1* (12), 2075–2081. https://doi.org/10.1002/celc.201402262.

(26) Binninger, T.; Mohamed, R.; Waltar, K.; Fabbri, E.; Levecque, P.; Kötz, R.; Schmidt, T. J. Thermodynamic Explanation of the Universal Correlation between Oxygen Evolution Activity and Corrosion of Oxide Catalysts. *Sci Rep* **2015**, *5* (1), 12167. https://doi.org/10.1038/srep12167.

(27) Wuttig, A.; Surendranath, Y. Impurity Ion Complexation Enhances Carbon Dioxide Reduction Catalysis. *ACS Catal.* **2015**, *5* (7), 4479–4484. https://doi.org/10.1021/acscatal.5b00808.

(28) Smith, G.; Dickinson, E. J. F. Error, Reproducibility and Uncertainty in Experiments for Electrochemical Energy Technologies. *Nat Commun* **2022**, *13* (1), 6832. https://doi.org/10.1038/s41467-022-34594-x.

(29) Bell, S. *Good Practice Guide No. 11. The Beginner's Guide to Uncertainty of Measurement (Issue 2)*; National Physical Laboratory, 2001.

(30) Miller, J.; Miller, J.; Miller, R. *Statistics and Chemometrics for Analytical Chemistry*, Seventh Edition.; Pearson Education: Harlow, England, 2018.

(31) Chen, R.; Yang, C.; Cai, W.; Wang, H.-Y.; Miao, J.; Zhang, L.; Chen, S.; Liu, B. Use of Platinum as the Counter Electrode to Study the Activity of Nonprecious Metal Catalysts for the Hydrogen Evolution Reaction. *ACS Energy Lett.* **2017**, *2* (5), 1070–1075. https://doi.org/10.1021/acsenergylett.7b00219.

(32) Kawashima, K.; Marquez, R. A.; Son, Y. J.; Guo, C.; Vaidyula, R. R.; Smith, L. A.; Chukwuneke, C.; Mullins, C. B. Accurate Potentials of Hg/HgO Electrodes: Practical Parameters for Reporting Alkaline Water Electrolysis Overpotentials. *ACS Catal.* **2023**, *In Press*.

(33) Jerkiewicz, G. Standard and Reversible Hydrogen Electrodes: Theory, Design, Operation, and Applications. *ACS Catal.* **2020**, *10* (15), 8409–8417. https://doi.org/10.1021/acscatal.0c02046.

(34) Feltham, A. M.; Spiro, M. Platinized Platinum Electrodes. *Chem. Rev.* **1971**, *71* (2), 177–193. https://doi.org/10.1021/cr60270a002.

(35) Zheng, W.; Liu, M.; Lee, L. Y. S. Best Practices in Using Foam-Type Electrodes for Electrocatalytic Performance Benchmark. *ACS Energy Lett.* **2020**, 3260–3264. https://doi.org/10.1021/acsenergylett.0c01958.

(36) Anantharaj, S.; Kundu, S. Do the Evaluation Parameters Reflect Intrinsic Activity of Electrocatalysts in Electrochemical Water Splitting? *ACS Energy Lett.* **2019**, *4* (6), 1260–1264. https://doi.org/10.1021/acsenergylett.9b00686.

(37) Morales, D. M.; Risch, M. Seven Steps to Reliable Cyclic Voltammetry Measurements for the Determination of Double Layer Capacitance. *J. Phys. Energy* **2021**, *3* (3), 034013. https://doi.org/10.1088/2515-7655/abee33.

(38) Mata, A.; Fleischman, A. J.; Roy, S. Characterization of Polydimethylsiloxane (PDMS) Properties for Biomedical Micro/Nanosystems. *Biomed Microdevices* **2005**, *7* (4), 281–293. https://doi.org/10.1007/s10544-005-6070-2.

(39) Raj M, K.; Chakraborty, S. PDMS Microfluidics: A Mini Review. *J. Appl. Polym. Sci.* **2020**, *137* (27), 48958. https://doi.org/10.1002/app.48958.

(40) Kawashima, K.; Márquez-Montes, R. A.; Li, H.; Shin, K.; Cao, C. L.; Vo, K. M.; Son, Y. J.; Wygant, B. R.; Chunangad, A.; Youn, D. H.; Henkelman, G.; Ramos-Sánchez, V. H.; Mullins, C. B. Electrochemical Behavior of a Ni3N OER Precatalyst in Fe-Purified Alkaline Media: The Impact of Self-Oxidation and Fe Incorporation. *Mater. Adv.* **2021**. https://doi.org/10.1039/D1MA00130B.

(41) Hall, D. S.; Bock, C.; MacDougall, B. R. An Oxalate Method for Measuring the Surface Area of Nickel Electrodes. *J. Electrochem. Soc.* **2014**, *161* (12), H787. https://doi.org/10.1149/2.0711412jes.

(42) Bode, H.; Dehmelt, K.; Witte, J. Zur Kenntnis Der Nickelhydroxidelektrode—I.Über Das Nickel (II)-Hydroxidhydrat. *Electrochimica Acta* **1966**, *11* (8), 1079–1087. https://doi.org/10.1016/0013-4686(66)80045-2.

(43) Lyons, M. E. G.; Brandon, M. P. The Oxygen Evolution Reaction on Passive Oxide Covered Transition Metal Electrodes in Aqueous Alkaline Solution. Part 1-Nickel. *Int. J. Electrochem. Sci.* **2008**, *3*, 39.

(44) Dionigi, F.; Strasser, P. NiFe-Based (Oxy)Hydroxide Catalysts for Oxygen Evolution Reaction in Non-Acidic Electrolytes. *Adv. Energy Mater.* **2016**, *6* (23), 1600621. https://doi.org/10.1002/aenm.201600621.

(45) Corrigan, D. A. The Catalysis of the Oxygen Evolution Reaction by Iron Impurities in Thin Film Nickel Oxide Electrodes. *J. Electrochem. Soc.* **1987**, *134* (2), 377. https://doi.org/10.1149/1.2100463.

(46) Wang, Z.; Murphy, A.; O'Riordan, A.; O'Connell, I. Equivalent Impedance Models for Electrochemical Nanosensor-Based Integrated System Design. *Sensors* **2021**, *21* (9), 3259. https://doi.org/10.3390/s21093259.

(47) Harrington, D. A.; Conway, B. E. Ac Impedance of Faradaic Reactions Involving Electrosorbed Intermediates—I. Kinetic Theory. *Electrochimica Acta* **1987**, *32* (12), 1703–1712. https://doi.org/10.1016/0013-4686(87)80005-1.

(48) Lyons, M. E. G.; Brandon, M. P. The Significance of Electrochemical Impedance Spectra Recorded during Active Oxygen Evolution for Oxide Covered Ni, Co and Fe Electrodes in Alkaline Solution. *J. Electroanal. Chem.* **2009**, *631* (1), 62–70. https://doi.org/10.1016/j.jelechem.2009.03.019.

(49) Garcia, A. C.; Touzalin, T.; Nieuwland, C.; Perini, N.; Koper, M. T. M. Enhancement of Oxygen Evolution Activity of Nickel Oxyhydroxide by Electrolyte Alkali Cations. *Angew. Chem. Int. Ed.* **2019**, *58* (37), 12999–13003. https://doi.org/10.1002/anie.201905501.

(50) Armstrong, R. D.; Henderson, M. Impedance Plane Display of a Reaction with an Adsorbed Intermediate. *J. Electroanal. Chem. Interfacial Electrochem.* **1972**, *39* (1), 81–90. https://doi.org/10.1016/S0022-0728(72)80477-7.

(51) Niu, S.; Li, S.; Du, Y.; Han, X.; Xu, P. How to Reliably Report the Overpotential of an Electrocatalyst. *ACS Energy Lett.* **2020**, *5* (4), 1083–1087. https://doi.org/10.1021/acsenergylett.0c00321.